A Passive Infrared Ice Detection Technique for Helicopter Applications

Adam L. Dershowitz
R. John Hansman, Jr.

Aeronautical Systems Laboratory
Department of Aeronautics & Astronautics
Massachusetts Institute of Technology
Cambridge, Massachusetts USA

August 20, 1991

ASL-91-4

Abstract

A technique has been developed, and successfully tested, to detect icing remotely on helicopter rotor blades. Using passive infrared (IR) thermometry it is possible to detect the warming caused by latent heat released as supercooled water freezes. During icing, the ice accretion region on the leading edge of the blade is found to be warmer than the uniced trailing edge resulting in a chordwise temperature profile characteristic of icing. Preliminary tests, using an IR Thermal video system, were conducted on a static model in the NASA Icing Research Tunnel (IRT) for a variety of wet (glaze) and dry (rime) ice conditions. A prototype detector system was built consisting of a single point IR pyrometer, and experiments were run on a small scale rotor model. Using this prototype detector the characteristic chordwise temperature profiles were again observed for a range of icing conditions. Several signal processing methods were investigated, to allow automatic recognition of the icing signature. Additionally, several implementation issues were considered. Based on both the static and subscale rotor tests, where ice was successfully detected, the passive IR technique appears to be promising for rotor ice detection.

This document is based on the thesis of Adam L. Dershowitz submitted in partial fulfillment of the degree of Master of Science in Aeronautics and Astronautics at the Massachusetts Institute of Technology.

Acknowledgements

This work was supported by the National Aeronautics and Space Administration, Lewis Research Center and the U.S. Army under grant NAG 3-927. The authors would also like to thank the B.F. Goodrich Company and the Douglas Aircraft Company for their cooperation during the IRT tests and Professor Ken Dewitt and Alan Yaslick for providing the thermocouple data.

Contents

Nomenclature

A_d	Detector Area
D^*	Relative Detector Sensitivity
D	Distance from Target to Detector
e	Emissivity
P	Incident Power
V_n	Noise Voltage
V_s	Signal Voltage
Δf	Detector Bandwidth

1. Introduction

The reliable measurement of ice accretion is an important requirement for helicopter all-weather operation. Rotor icing can present a significant hazard due to several different effects. The change in airfoil shape can lead to significantly increased torque requirements, due to increased drag and aerodynamic performance degradation.[1] These effects, and uneven spanwise icing, can lead to control problems. Uneven icing, and more commonly, uneven ice shedding can lead to severe vibrations. Helicopter exposure to icing conditions has increased over the past decade due to the increase in routine instrument flight operations.

The two primary helicopter applications for ice detection are the monitoring of critical components for Caution and Warning alerts, and the management of ice protection systems. For Caution and Warning applications, ice accretion on critical components should be detected before a hazardous condition exists. This information must then be conveyed quickly and accurately to the pilot, to allow the pilot to reverse course, change altitude, land, or activate a deicing system, before a critical quantity of ice has accreted.

For helicopters equipped with ice protection systems, the management of these systems can be critical. The most common type of rotor protection is electrothermal deicing. These systems require significant amounts of electrical power so the blades are typically heated for deicing in segments.[2] Typically, in such a system, each blade segment is heated, using full available electrical power, for a preset time. In some cases the system has a high and low setting, but can not be optimized for the specific icing conditions. Because there are no effective rotor ice detection systems it is necessary to overheat and continually cycle the electrothermal deicing systems to assure adequate ice protection.

If effective ice detection were employed the deicing systems could be operated more efficiently and effectively. It would become possible to heat a section of the blade, only until ice shedding occurs, thereby conserving some of the limited supply of electrical power available or allowing the next section of blade to be deiced more quickly. Such a detection system would also provide warning of a deicing systems failure, or of flight into such extreme icing conditions that the deicing system is not able to function effectively.

Because rotating components often experience a significantly different icing condition than the fuselage, visual evidence of ice accretion on non-rotating structures is not adequate for Caution and Warning applications. Indirect indications of icing such as torque rise or vibration typically emerge only after the hazardous condition exists. Ideally, the direct measurement of ice accretion on the rotating components would provide the earliest and most accurate measurement of potential icing hazards.

This thesis is a discussion of research that has led to the construction and testing of a system that successfully provides early ice accretion warning. Chapter 2 provides some background of existing ice detection methods. Chapter 3 is a discussion of the theory of the infrared ice detection method that was developed. Proof of concept infrared ice detection experiments were run on a static airfoil. These tests, and their successful results, are discussed in chapter 4. The next stage in the development of the ice detection method was to design and build a prototype detector, to be run on a rotating system. A description of these experiments, and their effective results make up Chapter 5. Chapter 6 is a discussion of some of the many implementation issues that must be considered for the implementation of an infrared ice detection system on helicopters. Finally a conclusion is presented in Chapter 7.

2. Background

There are currently many different types of ice detectors in use, and most employ direct contact. There are problems in using these in helicopter rotor applications. However by measuring ice remotely, it is possible to overcome many of these problems.

2.1. Existing Ice Detection Techniques

The most common ice detectors currently employed for aviation applications are direct contact type devices. In contact type detectors either a probe or surface mounted transducer senses the ice presence through a variety of physical mechanisms. These include resonant frequency shifts, optical blocking, heat capacity, electrical capacitance, and ultrasonic thickness gauging.[3]

Contact type ice detectors have not been successfully utilized for direct measurement of rotor ice accretion due to the difficulties inherent in placing the instrument on the rotors. Structural limitations can make it difficult to cut the blade in order to mount the detectors. In addition, there are difficulties in transmitting the sensor information from the rotating to the non-rotating frame. Solutions such as slip rings may be used. However they add cost and complexity to the system and have signal quality problems. Some contact type detectors have acceleration limitations which may be exceeded when mounted on a rotor. Detector erosion is also a problem. As a result, contact type detectors are typically mounted on the fuselage and the rotor conditions are inferred.[4] This is sometimes done by aspirating the probe at the airspeed of some spanwise rotor location. These techniques have had limited success because of the complex dependence of the icing process on temperature, liquid

water content and velocity, which vary significantly between the fuselage and rotor, as well as along the blade span itself.

2.2. Remote Monitoring of Rotating Blades

Remote sensing offers significant advantages for monitoring rotating blades. If ice accretion can be remotely detected by sensors mounted in the fuselage, then a measurement of rotor ice accretion can be accomplished without the difficulties identified above. Several potential techniques have been investigated for remote ice detection including: high speed video, active IR (infrared), and active microwave. High speed video would allow the pilot to view the blade in stop action, however, it is not easy to visually detect thin or clear ice accretions. In principle it is possible to measure changes in signal strength, or phase, of reflected microwaves, optical, or infrared radiation to detect ice. However such systems would be complicated, and may have problems such as background noise, and atmospheric absorption. The technique which has emerged as the most promising is passive IR.

Passive IR video thermography has been used for several years in the U.S. and France as a diagnostic tool for validation of ice accretion modeling codes.[5,6] Synchronized IR video images have also been used to monitor rotating components in flight as part of the NASA Advanced Turboprop development effort.[7]

3. Theory of Passive Infrared Ice Detection

The passive infrared ice detection method allows remote measurements of ice accretion on the rotor blade, from the fuselage. It avoids many of the problems of contact type detectors, and can additionally be used to monitor deicing system performance. The theory of such a passive infrared system is as follows.

The passive IR technique detects ice accretion by detecting the warming of the blade leading edge during icing. This is accomplished through remote IR thermometry. When ice accretes on an airfoil or rotor, the region where the accretion occurs becomes warmer than the surrounding surface due to release of the latent heat of fusion as the impinging supercooled water droplets freeze.[8] This process is shown schematically in Figure 1. It should be noted that the ice accretion is typically limited to a small region near the leading edge, and that much of the rotor surface will remain clear of ice. These uniced areas will have surface temperatures at or near the ambient temperature which will always be below freezing in icing conditions.

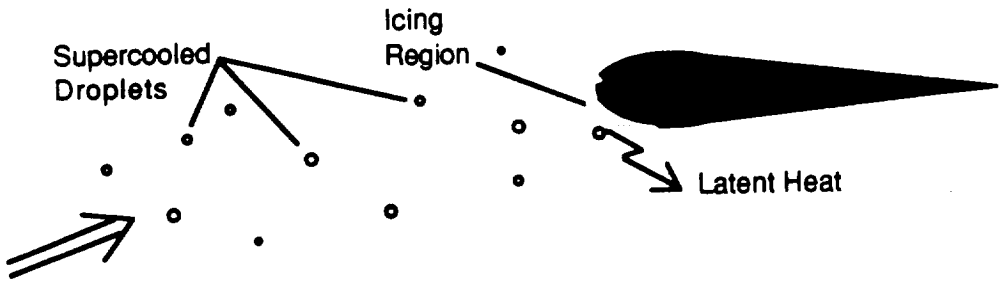

Figure 1 Schematic representation of latent heat release during icing

As a result of the thermodynamic processes described above, in icing conditions the rotors will exhibit a characteristic chordwise surface temperature profile, with the leading

edge significantly warmer than the trailing edge. Examples of schematic temperature profiles are shown in Figure 2 for wet and dry icing conditions. Prior to icing, the rotors will equilibrate to some temperature slightly warmer than the static air temperature due to kinetic heating. During icing, the temperature will increase in the accretion region as indicated in Figure 2. For wet (glaze) ice accretions, the wet zone, in the stagnation region, will remain at 0°C. This is due to the latent heat release which maintains the temperature at freezing until all the water has frozen. For dry (rime) accretions the temperature will reach a peak in the stagnation region at some temperature below freezing.

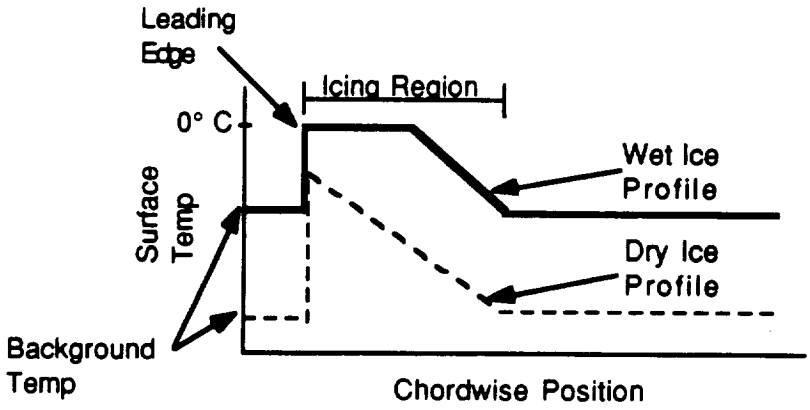

Figure 2. Schematic chordwise temperature profiles for wet and dry icing conditions

The characteristic temperature profile described above can be remotely measured by use of an infrared pyrometer. The spectrum of radiation emitted from a surface, and the intensity emitted, are a function of the surface temperature, and the emissivity.[9] Typical black body curves, for various temperatures, are shown in Figure 3.[10] As can be seen there is relatively little energy emitted from targets that are below freezing. An infrared pyrometer is essentially an infrared telescopes that focuses the incident radiation from a target on to an IR detector. By measuring the intensity of the radiation, within a given bandwidth, and knowing the emissivity of the target, it then becomes possible to infer the target surface

temperature. In this application the detector measures the surface temperature of the blade, or of the wet or dry ice accretion.

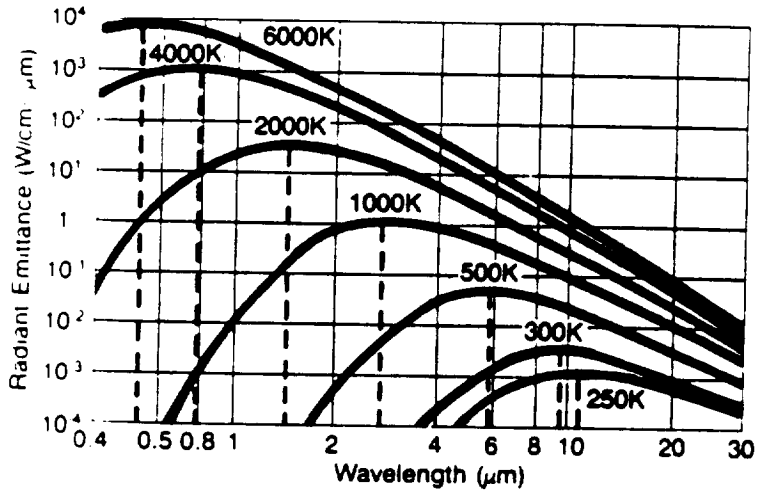

Figure 3. Black body emission curves for various temperatures

The passive IR system also has the potential to be used to monitor the operation of thermal deicing systems. As the detector measures only the surface temperature, it will measure the cold ice temperature during icing. When a thermal deicing system is activated, and enough heat is added to the blade, the ice will shed. The relatively hot blade surface will then be exposed, resulting in a significant increase in the thermal signature. This change in temperature profile can be used to indicate that successful deicing of the section has occurred, and the system can automatically cycle to other blade sections or shut down. Current thermal deicing systems are typically run assuming a worst case ice accretion, so they operate at high power for conservatively long times, resulting in unnecessary electrical load and excessive blade heating.

In one proposed implementation of passive IR ice detection, shown schematically in Figure 4, the rotor surface temperature would be measured by an infrared pyrometer

mounted on the fuselage and aimed up at the rotor plane. As the blade passed through the fixed field of view of the detector the effect would be to generate a chordwise blade scan. The aim point of such a detector could be varied between spanwise positions to give full coverage of the blade.

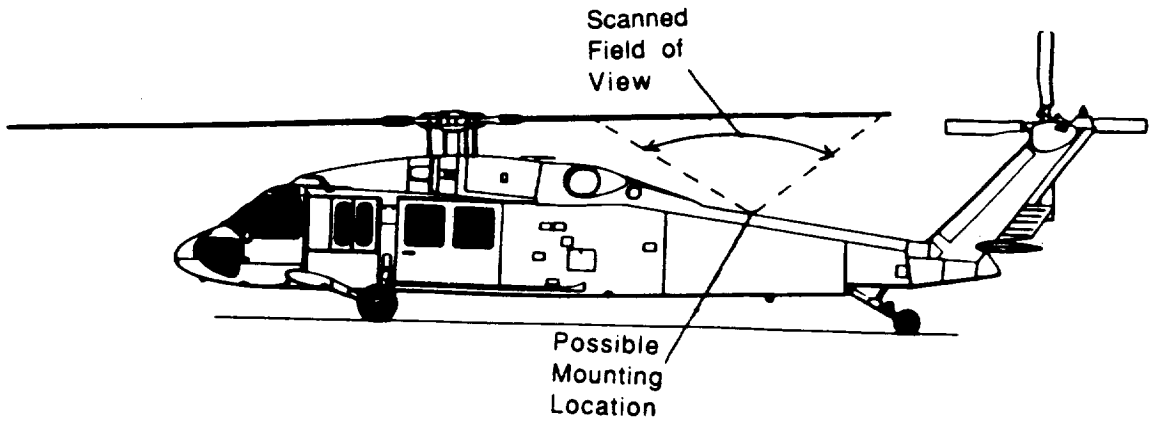

Figure 4. Possible helicopter mounting scheme for a passive infrared ice detector

Due to uncertainty in surface emissivity, attenuation through the icing cloud and thermal drift of the detectors it is sometimes difficult to accurately determine absolute surface temperature, however relative temperature resolution of 0.2°C is achievable.[11] This is considered adequate for ice detection where only the relative temperature profile between the leading and trailing edge regions is required.

4. Static Tests

Preliminary proof of concept experiments were run on a static airfoil in the NASA IRT (Icing Research Tunnel). The airfoil was observed using an infrared video camera. The expected temperature profiles, with a warmer leading edge, were observed during icing.

4.1. Experimental Setup for Static Tests

In order to evaluate the feasibility of the passive IR ice detection concept, a series of static tests were conducted in the NASA Icing Research Tunnel (IRT). These preliminary tests were conducted on a non-rotating 2 m (6 ft) chord airfoil model with a 25° sweep which could be varied between ±20° angle of attack. The model was instrumented with thermocouples and electrothermal heaters in the leading edge region.

Infrared imaging was accomplished using a Hughes Probeye thermal imaging system which used 6 Indium Antimonide (InSb) detectors and a spinning mirror arrangement to scan both horizontally and vertically. This production imaging system is somewhat more complex than that required for a simple ice detection system. The detectors used in this camera are sensitive in wavelengths from 2.0 to 5.6 microns. They are cooled using pressurized argon gas, which is allowed to expand, thus providing cooling. In the imaging system the output of the detectors was fed into a processor that developed thermal video images. Additionally the camera was able to calculate and display a graph of the temperature across a selected line from the image. This feature was useful, as it was possible to select and plot the chordwise temperature of the airfoil. The data from the IR camera was stored on videotape.

In the experimental set up, shown in Figure 5, the IR camera was mounted outside of the tunnel and viewed the leading 30 cm (11.8 in) of the airfoil through a hole in the tunnel window. This geometry led to some problems in calibration. Temperature gradients within the camera, resulting from the cold air blast, caused errors in the thermal compensation system resulting in a zero shift. However the relative temperatures measured were considered accurate.

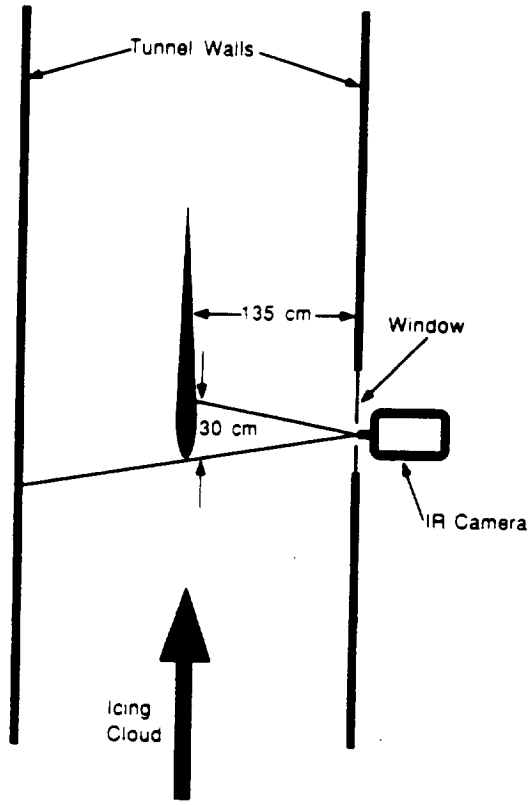

Figure 5. Schematic of IRT setup

4.2. Procedure for Static Tests

Experiments were run over a wide range of icing conditions, with airspeeds from 58 m/s (129 mph) to 93 m/s (208 mph) temperatures from -17°C (2.4 °F) to -3°C (26° F) and LWC (liquid water content) from 0.53 g/m^3 to 1.96 g/m^3. The spray bars in the IRT had

been calibrated, so that the pressures could be set to give a desired LWC, and MVD (mean volumetric diameter). For each experimental run, the airfoil was first cleared of any ice, using heating and scrapers. The airspeed and temperature of the wind tunnel were then stabilized. The spray was turned on for a predetermined time span, typically 1 to 3 minutes, then shut off. Data was recorded from video cameras, and from the IR camera, on video tape, and from the thermocouples by computer. After the airfoil and ice had returned to the equilibrium temperature, in some cases, the spray was cycled on a second time, for 30 seconds, without deicing first. This second cycle allowed verification of the ability of the technique to detect ice accretion over an existing ice layer. These additional tests showed no difference from cases with ice accretion over the airfoil skin itself. In some cases, after some ice has formed, the electro-thermal deicing system was cycled on to deice the airfoil. This heating cycle was monitored, and ice shedding was clearly indicated with the IR camera

4.3. Static Test Results

A pair of typical IR video images are presented in Figure 6 for the swept airfoil at a tunnel temperature of -11°C (12.2°F), an LWC of 0.17 g/m^3, with an MVD of approximately 15 microns, an angle of attack of 4°, and a free stream velocity of 92 m/sec (206 mph). The camera viewed approximately the leading 30 cm (11.8 in) of the airfoil. The chordwise profile is presented horizontally. The diagonal line is the leading edge. Forward of the leading edge the far wind tunnel wall is visible. Note that the chordwise temperature profile is shown across the bottom of the image, as calculated by the camera. With the spray off, the airfoil surface temperature was uniform at approximately the tunnel temperature as shown in the figure on the left. Several seconds after the spray was turned on, the increase in leading edge surface temperature, resulting from the latent heat release, became clearly visible and is shown in the figure on the right. After the spray was turned off, the leading edge cooled, over 5 to 10 seconds, back to ambient.

Figure 6. IR video output of model lower surface (T=-11°C,V=92 m/s, LWC=0.17 g/m^3)

The IR, and thermocouple measured chordwise temperature profiles for typical wet (glaze) icing conditions are presented in Figure 7. This data was recorded on videotape, from the IR camera. It was then digitized for analysis and display, and the profile that was calculated by the camera, is shown here. In this case the tunnel temperature was -5°C (23°F), the LWC was 1.95 g/m^3, with an MVD of 20 microns, the angle of attack was 10°, and the free stream velocity was 59 m/s (132 mph). With the spray off, the airfoil had a uniform indicated temperature, as shown. The warm temperature observed upstream of the stagnation point is an image of the warm tunnel wall behind the airfoil. When the spray was turned on, the expected surface temperature profile for wet growth was observed. The leading 8 cm of the airfoil indicated a surface temperature of 0°C (32°F) indicating wet ice growth. Aft of the wet region, the surface temperature dropped to the uniced value, as there is no ice growth there. The thermocouple readings were consistent with the IR measurements. When the spray was turned off the surface temperature again became uniform and returned to the equilibrium tunnel temperature. When the spray was cycled on again, the characteristic wet ice temperature profile returned.

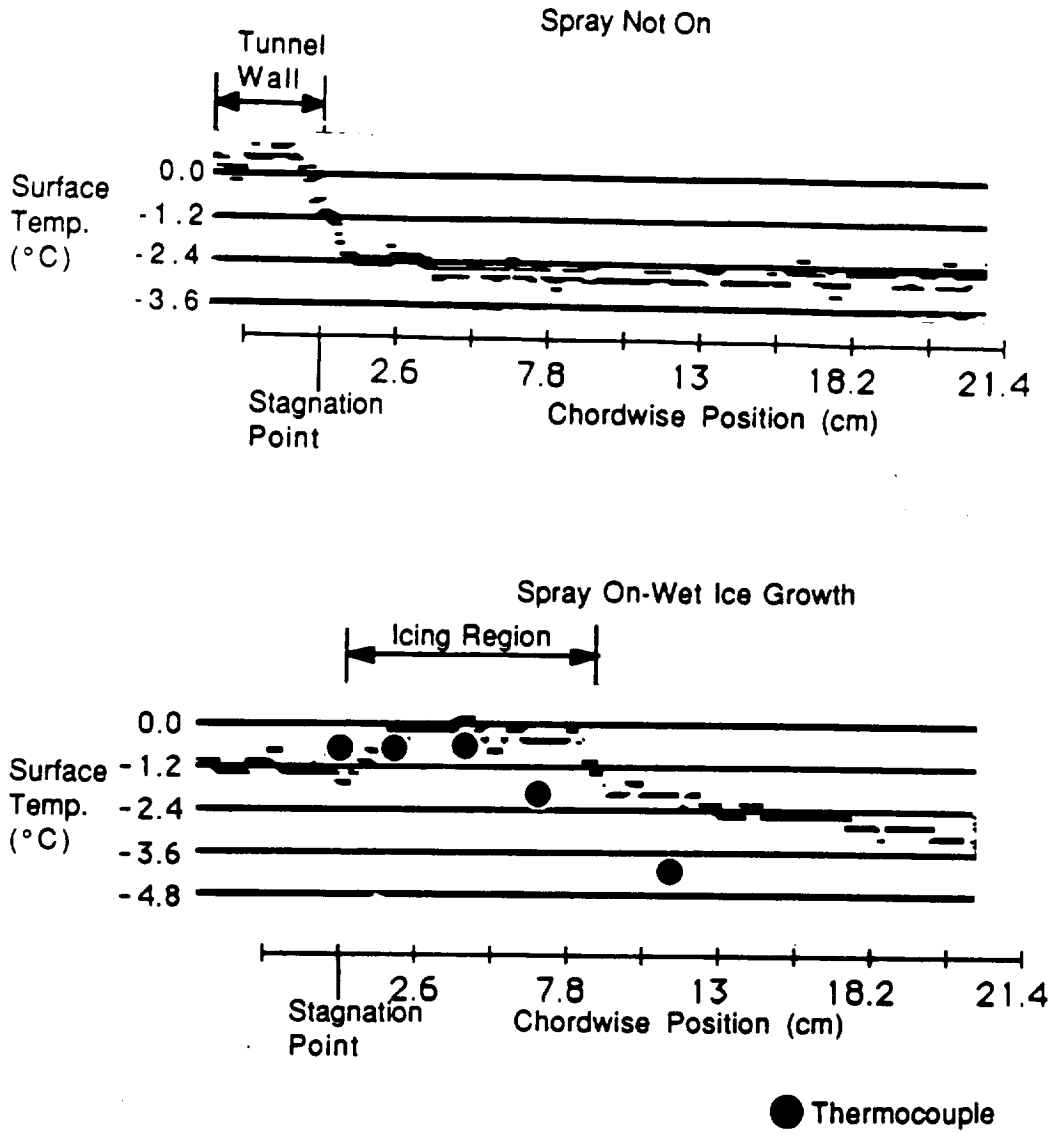

Figure 7. Chordwise temperature profiles for wet (glaze) ice conditions (T=-5°C, V=59m/s, LWC=1.95 g/m^3)

The IR measured temperature profiles for dry (rime) ice conditions also show the expected shape indicative rime of icing. An example is presented in Figure 8. In this case the tunnel temperature was -17°C (1.4°F), the LWC was 0.17 g/m^3 with an MVD of approximately 15 microns, the free stream velocity was 92 m/s (206 mph) and the angle of attack was 4.1°. With the spray off, the airfoil had a uniform indicated temperature. When

the spray was turned on, the surface temperature was seen to peak at the stagnation point. This curve is characteristic of dry (rime) growth where the surface temperature reflects the local collection efficiency (i.e. increased droplet impingement causes increased icing and increased heating). The stagnation point has the largest collection efficiency and consequently the greatest latent heat release. When the spray was turned off the temperature quickly dropped to the pre-icing value. The characteristic rime ice profile again appeared when the spray was cycled on.

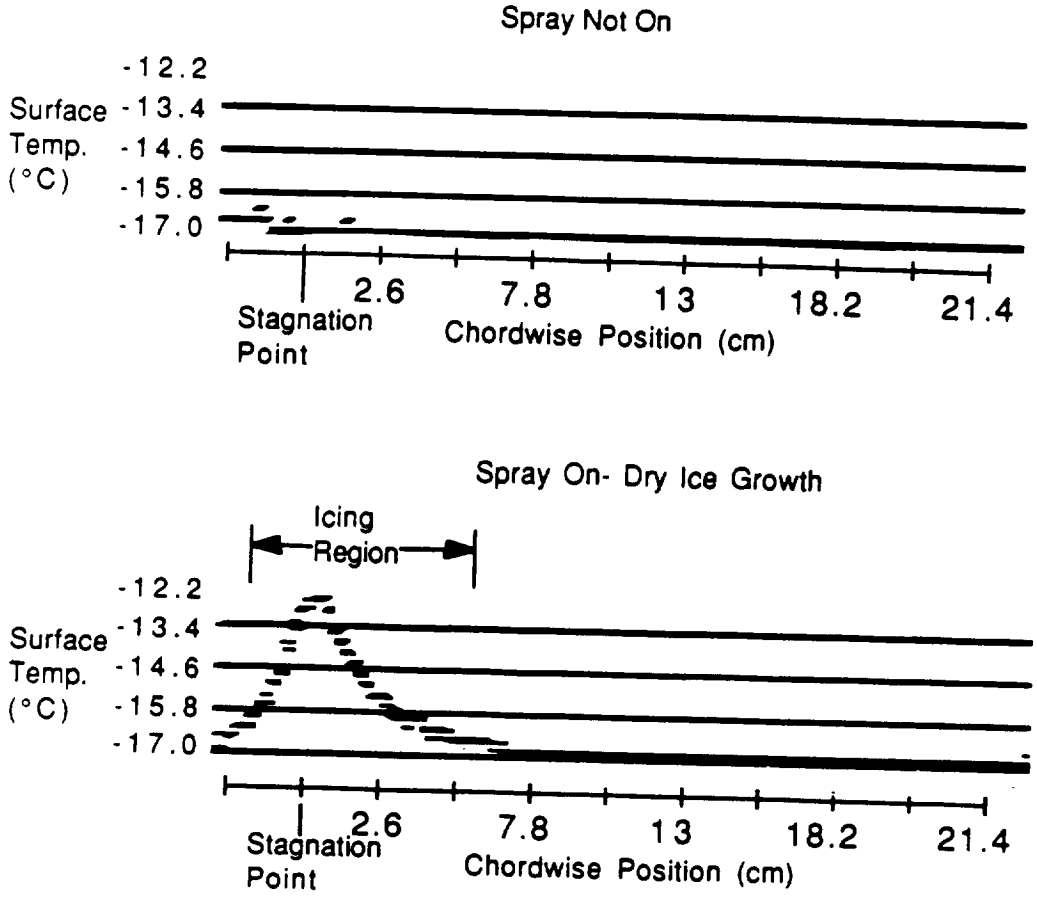

Figure 8. Chordwise temperature profiles for dry (rime) ice conditions (T=-17°C, V=92m/s, LWC=0.17 g/m^3).

The IR temperature profiles were also observed when the airfoil was electrothermally deiced. The ice warmed somewhat when the deicing elements were turned on, but before

the shedding event. When the ice was shed, the hot deicing elements were exposed. Shedding of ice was then apparent as a sudden significant increase in the surface temperature.

4.4. Lewice Results

Numerical simulations of the chordwise temperature profiles were also generated with the LEWICE ice accretion code. This code simulates ice growth numerically. It uses inviscid flow code to calculate particle trajectories.[12] In each region where the particles impinge on the airfoil an energy balance is calculated and used to determine the amount of ice that freezes out in that corresponding region, allowing ice growth simulation. As part of the energy balance the temperature in each impingement region is calculated.

The LEWICE code was run to simulate ice growth at the same conditions as were run in the IRT. The LEWICE predicted surface temperatures are consistent with those measured with the IR system. Figure 9 is a predicted temperature profile for the same airfoil and conditions as those measured and shown in Figure 7, as well as the measured profile. A comparison of these figures shows good agreement between the analytic results and the measured data.

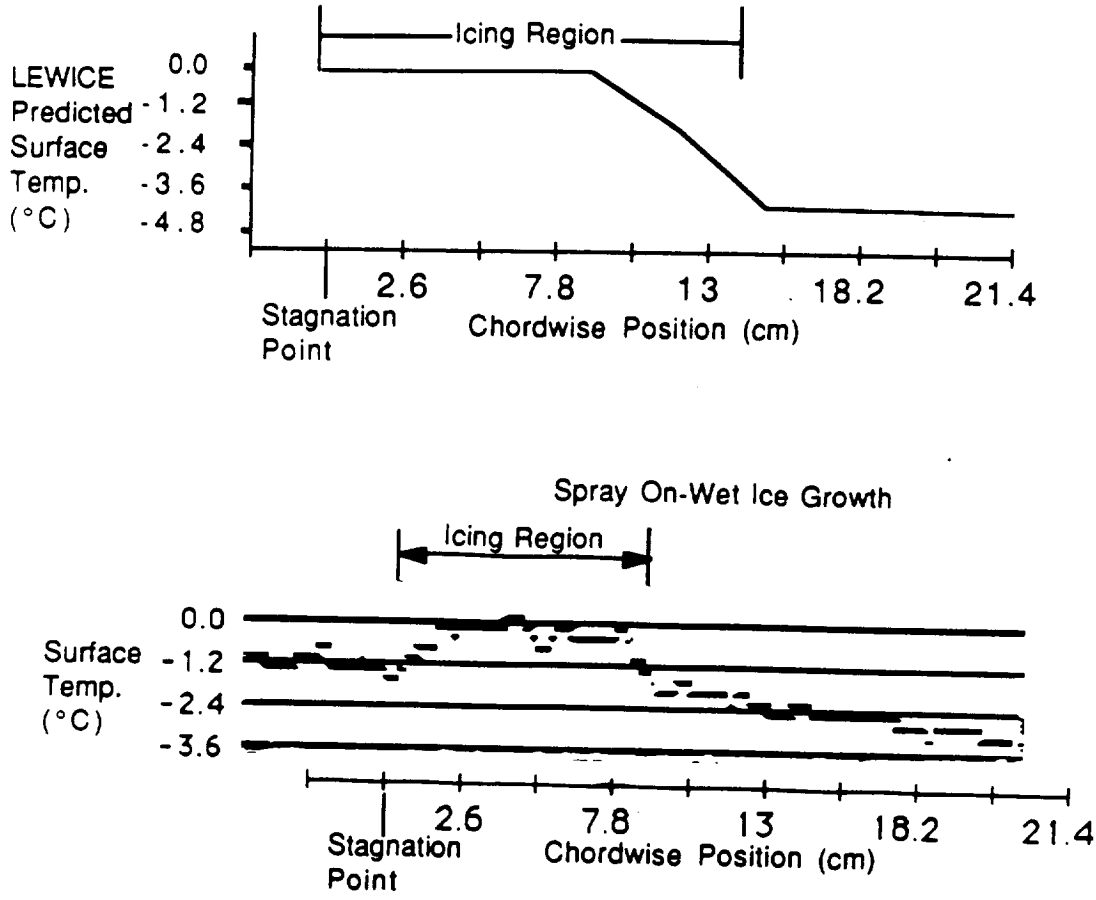

Figure 9. LEWICE predicted temperature profile for wet (glaze) ice conditions (T=-5°C, V=59m/s, LWC=1.95 g/m^3), and the measured profile.

Based on the good agreement between the LEWICE predicted and the observed temperature profiles, LEWICE was used to predict temperature profiles which could be expected for cases more representative of helicopter rotor conditions. An example is shown in Figure 10 for a 50 cm (19.7 in) chord NACA 0012 airfoil at 4° angle of attack and 76 m/s (170 mph) velocity. The freestream temperature was -17°C (1.4°F), and the LWC was 0.17 g/m^3, with a MVD of 25 microns. There is a slight temperature rise at the stagnation region due to ram heating that is more evident in the dry air conditions. The ram effect is localized because LEWICE does not include chordwise heat conduction in the airfoil. For the icing case, there is a significant temperature rise of approximately 6°C

(10.8°F) at the low LWC of 0.17 g/m^3. These LEWICE predictions indicate that the infrared ice detection techniques could be successful for helicopter rotor use.

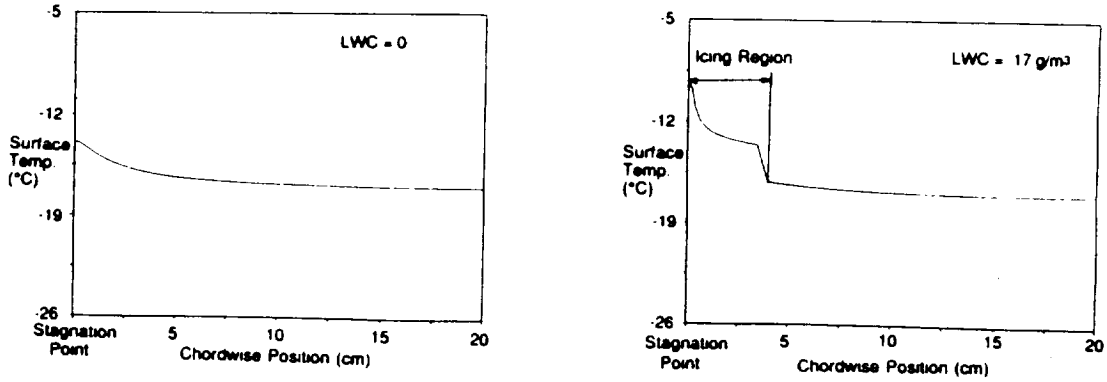

Figure 10 LEWICE predicted temperature profile for typical rotor conditions (T=-17°C, V=76m/s, LWC=0.17 g/m^3, chord=50cm).

5. Rotor Tests

The monitoring of a rotating blade involves some complications that are not present when monitoring a fixed blade. Because of these differences it was necessary to demonstrate that this same technique could be used in the rotating case. The static tests had successfully demonstrated the measurement concept. To follow up these experiments a detector, and a small scale rotor were built, and tests were run in the rotating configuration.

5.1. Infrared Ice Detector Design

In order to evaluate the IR ice detection technique on rotating systems a prototype detector, suitable for both flight and ground tests, was developed.[13] This ice detector, shown in Figure 11, is a point infrared pyrometer, essentially a telescope that operates in the infrared region. Other more complicated designs, in which the detector tracks with the blade, either mechanically or electronically (ie CCD's), to spend more time on the target point, thus boosting the integration time, were considered. The requisite significant increase in complexity did not appear to be worth the potential for increased, but unnecessary, performance.

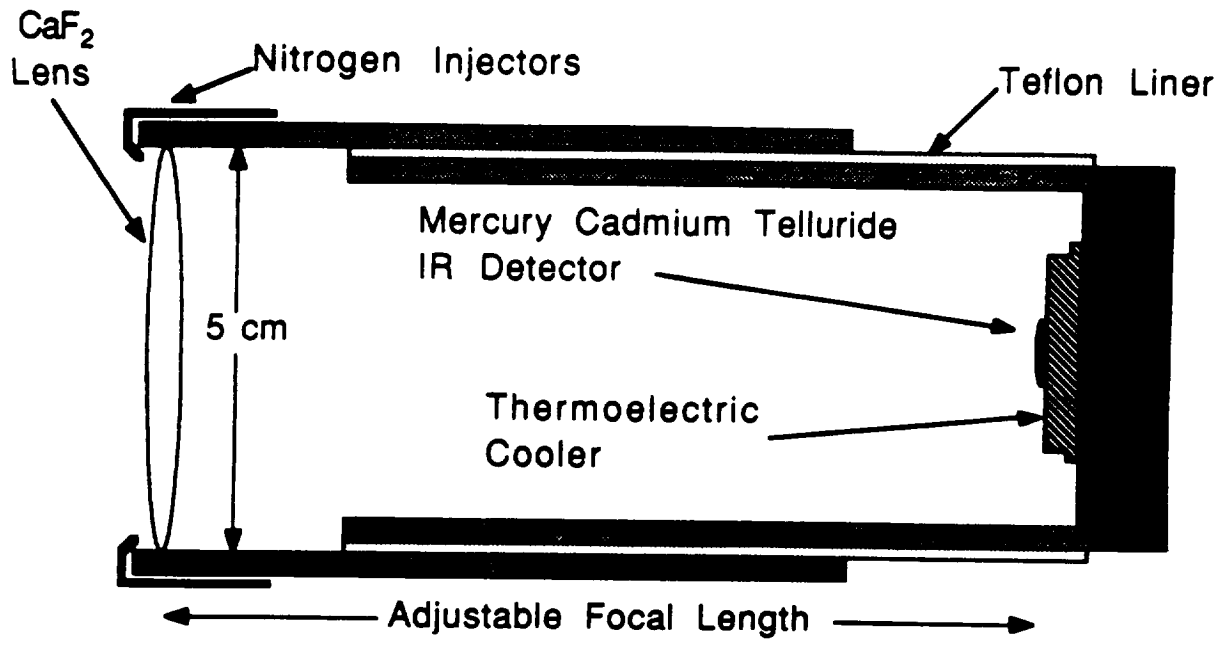

Figure 11. Infrared ice detector schematic

To specify the detector components, and to evaluate the applicability of existing infrared detectors, in terms of sensitivity, several assumptions were made. A typical main rotor has a chord length of 50 cm (19.7 in). The corresponding icing region is on the order of several centimeters. A target size of 1 cm diameter was deemed sufficient to detect ice on a typical rotor, thus allowing several detection samples within the icing region. A simple geometry for detector placement was assumed. The detector lens, and the target spot on the rotor were assumed to be parallel, and to be 2 m (78.7 in) apart. A lossless 0.002 m^2 (3.1 in^2) aperture was used to represent the optics, and all of the energy incident on the optics was assumed to focus down on to the detector. The target spot on the rotor was assumed to radiate as a black body (e=1.0) symmetrically into a hemisphere. The energy incident on the detector is thus a linear function of the aperture (lens) area, and of the target spot size, and decreases with D^2 (Distance from target to optics^2).

5.1.1. Infrared Detector Selection

The Stephan-Boltzman law for Black body radiation was used to calculate the incident energy on detectors with bandwidths of 0 to 5.5 microns and 0 to 11 microns at temperatures of 0°C (32°F) (typical case) and -20° C (-4°F) (worst case).[14] Typical detectors have a range of sensitivity of 1 to 5.5 microns, or 1 to 11 microns. The extra energy that would be added to the calculations by including the band from 0 to 1 microns is a very small amount of the total energy, so it was ignored. These assumed values predict the incident energy as shown in Table 1. As available detectors in the range 1 to 11 microns are over two orders of magnitude less sensitive than available detectors in the range 1 to 5.5 microns, the extra energy contained in the 5.5 to 11 microns was not worth the decreased sensitivity. Thus the shorter wavelength family of detectors was selected.

Temperature (°C)	Bandwidth (microns)	E emitted ($W \times 10^{-3}$)	E incident ($W \times 10^{-7}$)
-20°	0-11	4.08	3.3
-20°	0-5	0.140	0.11
0°	0-11	6.75	5.4
0°	0-5	0.327	0.26

Table 1. Incident energy on detector for various conditions

For design purposes the rotor blade was assumed to be 5.44 m (17.8 ft) long, 0.5 m (19.7 in) in chord, and to rotate at 28 radians/sec giving a tip velocity of 152.3 m/s (340 mph). For a 1 cm (0.39 in) target size a sampling time of 65.6 μs (15 kHz bandwidth=Δf) is necessary. A 30 kHz bandwidth was used, in this design, to provide more margin.

The figure of merit normally used to compare infrared detectors is D*, where

$$D^* = \frac{\sqrt{A_d \Delta f}}{P} \frac{V_s}{V_n}$$

D* is a relative measure of the sensitivity of the detectors. A larger D* corresponds to a higher sensitivity, or a larger signal to noise ratio (V_s/V_n) for a given incident power (P), and detector area (A_d).

As all the other values in this equation were known, from the geometric and temperature assumptions, for a given D* it was possible to calculate the expected signal to noise ratio V_s/V_n. Although InSb (Indium Antimonide) detectors offer high values of D* they must be cryogenically cooled. HgCdTe (Mercury Cadmium Telluride) detectors offer high D* values, and have the additional advantage that they can be thermoelectrically cooled, which is important for flight applications. This is because the cooling requirements are not as high, to obtain a given D* for HgCdTe. A typical HgCdTe detector (ie EG&G Judson J15TE4:5 HgCdTe) has a D* of 4×10^{10}, at a cooling temperature of -73°C (-99° F), which can be attained thermoelectrically.[15]. This D* gave a calculated signal to noise ratio of 10,161 at the assumed conditions and a target temperature of -20°C (-4°F). This was deemed sufficiently high to employ this detector, even considering the idealized assumptions that were made. Consequently an EG&G Judson J15TE4:5 HgCdTe detector was used in the prototype detector.

The HgCdTe detector that was used was manufactured already mounted in a package containing a four stage thermoelectric cooler. This thermoelectric cooler, with an external automatic temperature controller, keeps the temperature of the detector at -73°C (-99°F).

5.1.2. Ice Detector Optical Design

It was found that a single lens design, using a 100 mm (3.9 in) focal length lens, in which the lens was able to be moved relative to the detector, would allow enough range in focus for either lab tests or full scale flight tests. Additional lenses, used to make a compound optical design, would have increased the total signal absorption, so were not used.

There are many available lens materials that offer low absorption in the necessary infrared band. However these materials tend to be water soluble, or sensitive to thermal shock. These properties tend to prevent their use in an ice detection application. CaF_2 (Calcium Floride) offered a good balance. It is not particularly sensitive to water or thermal shock, and has low IR absorption in the required band, so it was chosen for the lens material.[16] Long term water damage to CaF_2 will occur however, so CaF_2 lenses would not be appropriate for production ice detector applications, unless the optics were protected from the icing environment.

5.2. Infrared Ice Detector: Mechanical and Electrical Design

The HgCdTe detector is positioned at the focus of a single biconvex CaF_2 lens, as is shown in Figure 11. Concentric aluminum tubes were used to make the case for the pyrometer, and to hold the detector and optics in place. A Teflon sleeve, between the tubes, allowed the length of the pyrometer to be adjusted giving a focus for a target distance ranging from 15 cm (5.9 in) to infinity. This range allowed the prototype to be used on a small test rotor in the lab or in full scale flight tests. This lens gave the detector a target spot

size of 0.18 cm (0.07 in) diameter at 56 cm (22 0 in) as used in some of the tests, and a spot size of 1 cm (.39 in) diameter at 3 m (118 in), which is more typical of the distance used for a helicopter application. In order to prevent icing or fogging of the lens three small tubes were set up to spray dry nitrogen across the lens. Although these gas jets did not completely prevent fogging in all cases, they did significantly decrease it.

The pyrometer was mounted in a bracket. This setup, shown in Figure 12, allowed a flat surface for mounting the detector. Additionally the focus could be adjusted by turning the focus wheel. This wheel rotated around the threaded rod, connected to the base of the detector. The threaded rod could thus move the base plate, and the inner tube of the detector. The friction in the system maintained the desired focus position.

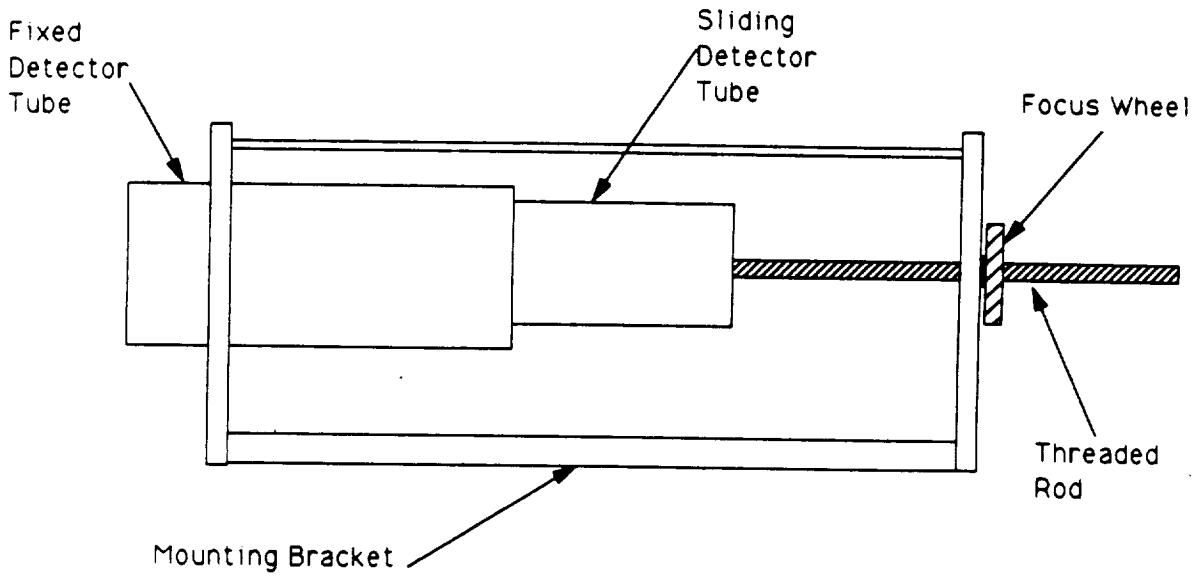

Figure 12. Pyrometer mounting bracket

5.2.1. Ice Detector Signal Processing

The signal from the pyrometer itself was processed as shown in Figure 13. It was first fed into a high gain, low noise amplifier. This amplifier additionally provided the bias

necessary for the detector. Therefore the amplifier was run on a gel cell battery avoiding the introduction of electrical power supply noise. The amplifier was AC coupled to prevent saturation. This had the effect of amplifying only short term temperature changes, while rejecting any DC bias. The detector could thus not be used to measure absolute temperature, but only relative temperature, over short time scales. The signal was sent into a digital oscilloscope, and stored making it possible to read this signal into a computer for post processing, if required.

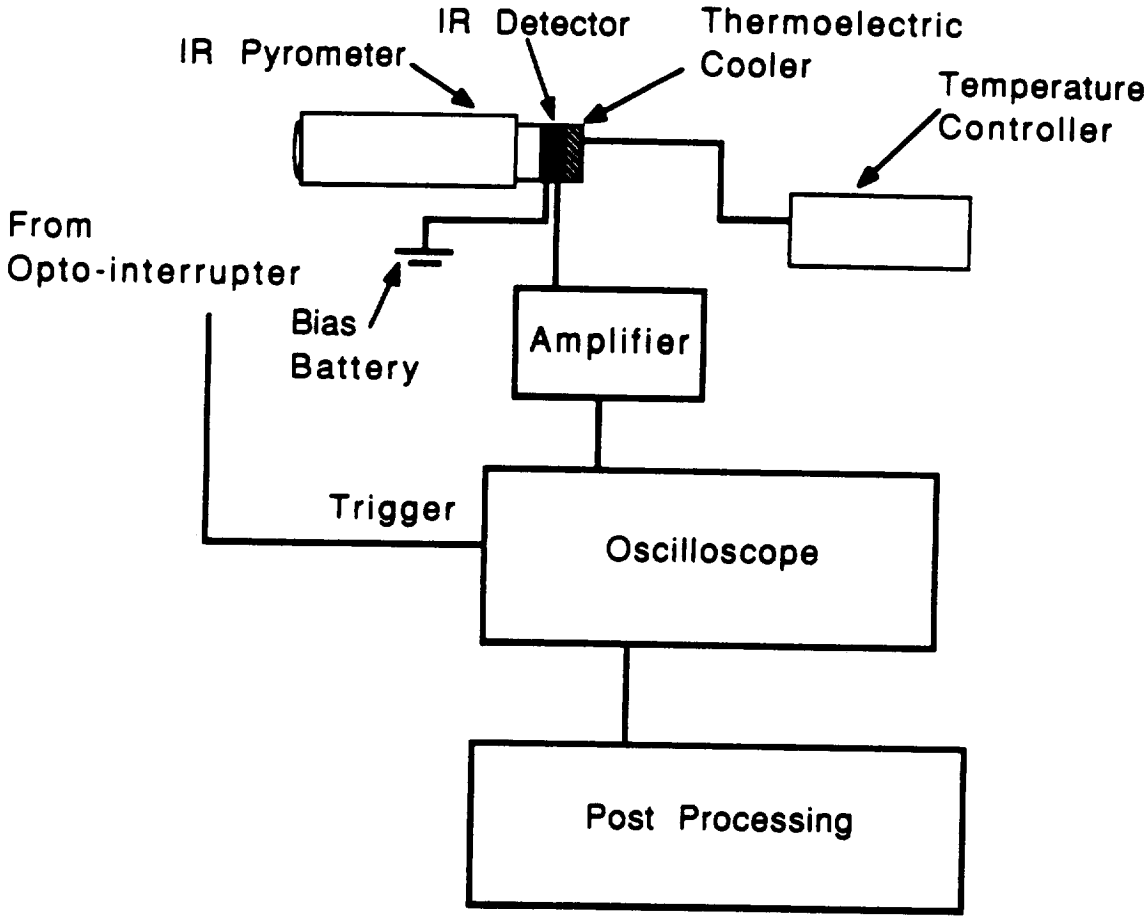

Figure 13. Ice detector signal processing path

5.3. Test Rig For Rotating Tests

In order to test the prototype ice detector, a test rig was constructed. It consisted of a counter-balanced single blade rotor with a 22 cm (8.66 in) span and a 2 cm (0.78 in) chord, built of solid aluminum, shown schematically in Figure 14. The airfoil section approximated a NACA 0012. The blade and counter balance were mounted directly on the shaft of an electric motor, through a locking joint that allowed different angles of attack to be set. The motor was mounted horizontally on a test stand, so the rotor axis was also horizontal. The small rotor was chosen to allow the entire rig to be placed in a lab freezer; the horizontal mounting allowed the largest possible separation between the detector and the rotor in the available freezer space. A top-opening 0.26 m^3 (9 $ft^{3)}$ freezer that was able to maintain temperature down to -23°C (-9.4°F) was used. This system was able to run over a range of rotation speeds, from 0 to 40 Hz.

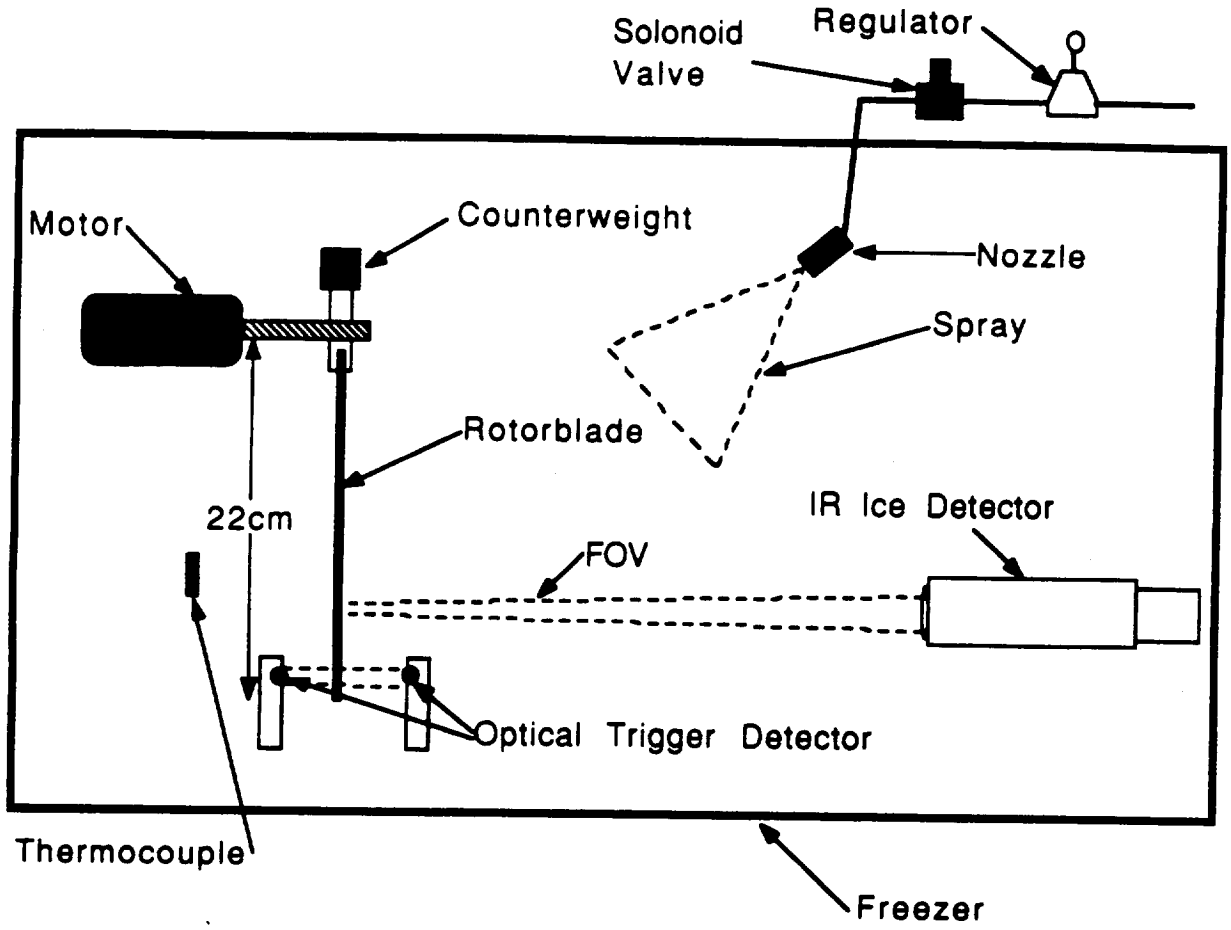

Figure 14. Rotor test rig

The tests were nominally run at 22 Hz which allowed good ice formation at reasonable rotor Reynolds numbers. The detector was aimed at a location 18 cm (7.1 in) from the center of the rotor, giving Reynolds numbers in the range of 4×10^4, although these varied with temperature. The blade passed through the field of view of the detector in 0.8 ms. This time is more typical of a tail rotor, while blade passage times for a main rotor are typically 6 ms. This test therefore was conservative in that significantly faster detector dynamics were required than would be necessary for main rotor use.

An opto-interrupter was set up across the blade to measure rotation rate and to provide trigger pulses for tracking the blade. It consisted of a light emitting diode, on one side of

the blade, and a phototransistor on the opposite side. When the blade passed, it interrupted the light path, thus switching the phototransistor, and sending out a trigger signal to the oscilloscope, and to a frequency counter.

The rotor and ice detector were both mounted in the freezer. The lens was 38 cm (15.0 in) from the rotor plane. The detector viewed the pressure surface of the blade, as in the proposed helicopter application. A hot focusing target was located behind the rotor blade, to position the detector. The ice detector was focused to provided the sharpest signal profile possible, using the change between the hot target, and the cool blade leading edge. The freezer temperature was measured using a thermocouple. It was mounted on the rotor test stand, just behind the rotor. To protect the thermocouple from icing, it was put in a copper tube, which was in turn wrapped with insulation, to limit heating due to the formation of ice on the tube.

5.3.1. Spray setup

Tap water was used for the spray system, as shown in Figure 15. A water pressure regulator was used to set the desired pressure. A solenoid valve, outside of the freezer, was used to turn the water flow on and off. The pressure regulator was set to the desired pressure. The water tube, which then led into the freezer, was partially wrapped in insulation, to prevent freezing, although in some cases the nozzle did freeze. In these cases the nozzle was defrosted, and the measurements were repeated. The nozzle was mounted approximately 20 cm (7.87 in) from the plane of the rotor, and near the center and top of the freezer. Due to space constraints it was necessary to mount it on the pressure side of the rotor.

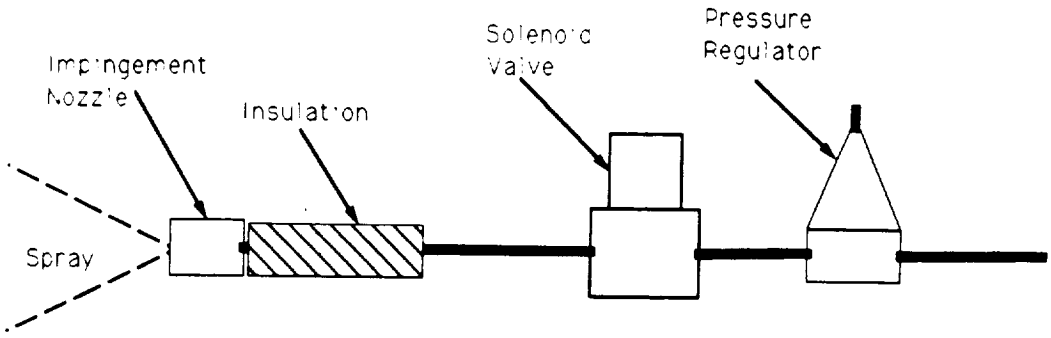

Figure 15 Spray setup schematic

Two different commercial spray nozzles were employed, to obtain different LWC values. These nozzles had a small spray orifice to provide the fluid stream. The stream was then atomized by impingement on a wire in front of the orifice, providing a fairly fine spray. Although the MVDs were not directly measured, the manufacturer claims that they "generate a high percentage of particles under 50 microns".[17] The LWC from the nozzles was estimated by first setting the water pressure, then mounting the nozzle 1 m (39 in) above a surface, and measuring the area that was sprayed. At that distance from the nozzle, the spray pattern was effectively circular. The particles were assumed to fall at 10 m/s (32.8 ft/s) to estimate the volume spray rate. Finally the water flow rate was measured. The spray volume rate divided by the flow rate yielded the estimated LWC, for each nozzle, at the given pressure setting. The smaller nozzle was run at 50 psi (344.7 kPa) an gave an estimated LWC of 0.17 g/m^3, while the larger nozzle was run at 30 psi (206.8 kPa) and gave an estimated LWC of 0.74 g/m^3.

5.4. Experimental Procedure

For a typical experimental run, the blade rotation rate and freezer temperature were allowed to stabilize. The temperature and rotation rate were recorded. An uniced

temperature profile was then recorded 10 seconds prior to spray initiation. The spray was turned on for 10 seconds. At the end of this cycle a temperature profile was recorded. Additional profiles were recorded 10 seconds later, and 20 seconds after that, when the blade had returned to an equilibrium state. Again the temperature and rotation rate were recorded. Finally the blade was deiced and the cycle was repeated. These runs were done over a range of temperatures from -20° C (-4°F) to 60° C (76°F), and at 0°, 5° and 10° angle of attack. During icing the rotation rate would drop slightly due to the increased drag from the ice, and the temperature would rise due to the latent heat release from the liquid water in the freezer freezing out. For the majority of the data collected the freezer was first cooled down to -22°C (-7.6°F), and allowed to stabilize. The spray nozzle was put in, and the freezer was then unplugged. Data was collected as the freezer gradually warmed up. Having the freezer turned off had the additional benefit of avoiding the electrical noise that the freezer motor would sometimes generate.

Typical profiles, for a cold case (T=-17.2°C), are shown in Figure 16. The curve on the left was measured before the spray was turned on, while the curve on the right was measured during the icing.

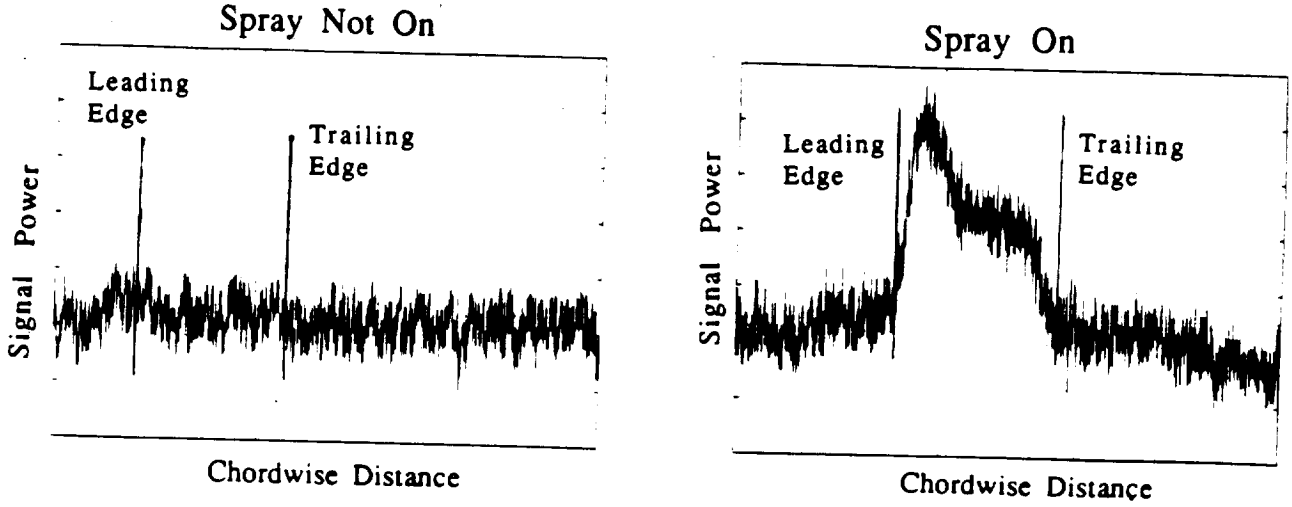

Figure 16. Example of unfiltered IR profiles.

As can be seen there is a significant amount of high frequency noise present. A digital low pass fifth order Butterworth filter with a cut off at 10 kHz was used to remove the high frequency noise from the digitized data after it was stored in the oscilloscope. Figure 17 shows the same pair of signals as in the prior figure, after being filtered. In the following, all IR signals are filtered, except where noted.

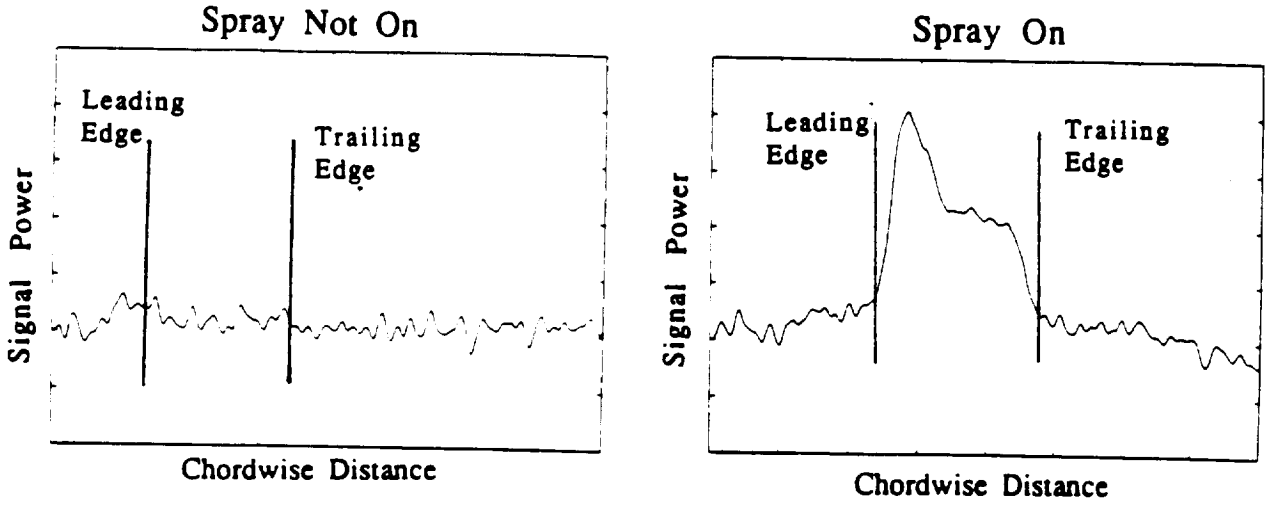

Figure 17. Example of filtered IR profile

The signals are presented in consistent arbitrary units. The IR signal amplitude is a function of many factors including amplifier gain, detector bias voltage, and distance to the target. Because icing is indicated by a change in the relative temperature, and in the profile shape, it was not necessary to calibrate an absolute temperature measurement. However to make it easier to compare different cases, the amplitude scales are all the same for all of the results presented below.

5.6. Results of Rotor Icing Tests

Figure 19 is an example of IR measured temperature profiles for cold conditions. The conditions for this case are a temperature of -17.2° C (1.0°F), 5° angle of attack, a rotation rate of 22 Hz and an LWC of 0.17 g/m^3. Before the spray was turned on, the rotor blade,

and the freezer wall were all at the same temperature, as indicated by the relatively flat line in the left graph. When the spray was turned on, as expected, the blade leading edge was heated by the latent heat release, and the characteristic dry (rime) icing chordwise temperature profile can be seen in the right graph of Figure 18. The region before the leading edge passage and after the trailing edge is the background, in this case the freezer wall. The relatively sharp temperature spike, with a peak at the stagnation point is characteristic of cold (rime) icing growth. The supercooled water freezes on contact with the surface, and the temperature profile approximately follows the local collection efficiency.

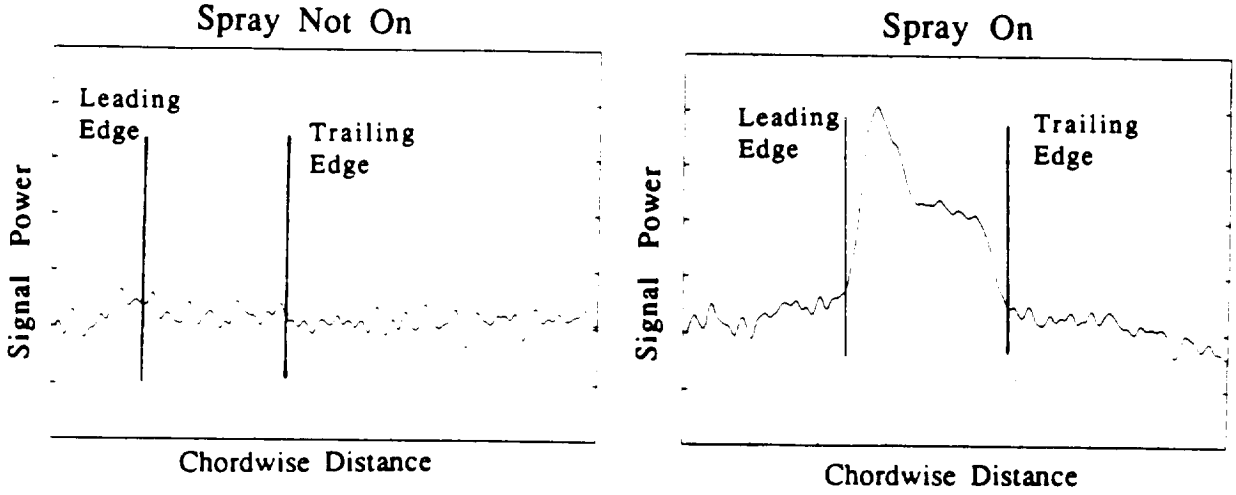

Figure 18. Cold IR profiles (T=-17.2°C)

Figure 19 is an example of a warmer ice accretion, where all the conditions are the same as the prior case except T=-9.1°C (15.6°F). Note the smaller signal amplitude. This is due to the warmer conditions, along with a maximum temperature of 0° C (32°F), so the temperature rise is more tightly bounded. As this limit is reached the icing region becomes somewhat flatter than in the prior case. The distinct icing profile is still present.

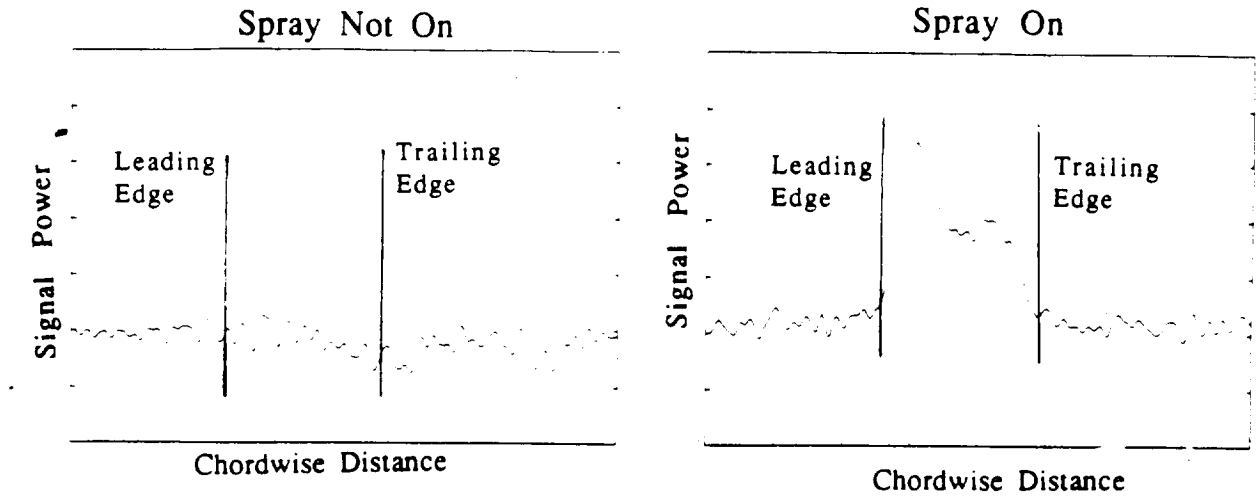

Figure 19. Warmer IR profiles (T=-9.1°C)

Because the relative temperature difference between the ice and the ambient blade temperature is lower during warm, glaze, ice accretion, this represents the most difficult conditions for the IR technique. Figure 20 again shows a similar case, but here the temperature had warmed to T=-1.8 °C (26°F) resulting in minimal ice formation, thus the small magnitude of the icing signal. In a glaze case, such as this, the highest possible temperature that can be maintained during icing is 0° C(32°F), due to latent heat release. When this occurs there is some liquid water present on the surface. This water can sometimes run back from the impingement region and result in runback icing. During glaze icing the chordwise temperature profile is flat in the impingement region, where the water load is highest, instead of displaying a temperature spike that is characteristic of rime icing. There is only a very slight amount of glaze ice formation at T=-0.9°C (30.3°F). Yet in Figure 21 there is still some icing indicated. In the left figure, before the spray was turned on, the blade was at a slightly reduced temperature from that of the background. When the rotor was stopped and observed in this case, there was a slight layer of glaze ice present. Finally at T=-0.3°C (31.5°F) no ice growth was observed. The signals in Figure 22 are both flat. There was essentially no change between the spray and prespray profiles demonstrating that the technique does not give false indications.

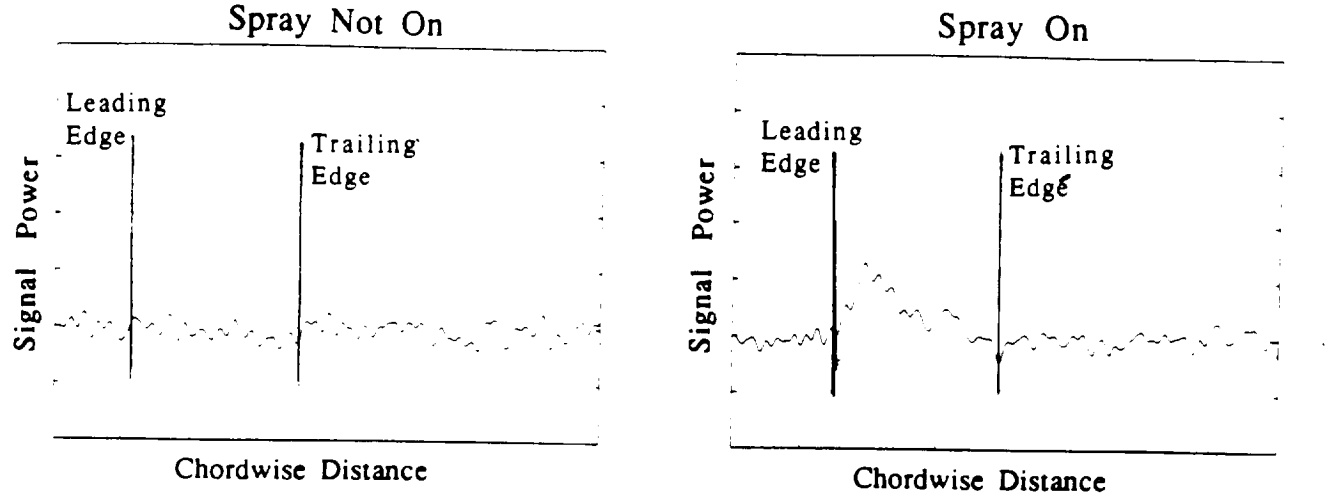

Figure 20 IR profiles at T=-1.8° C

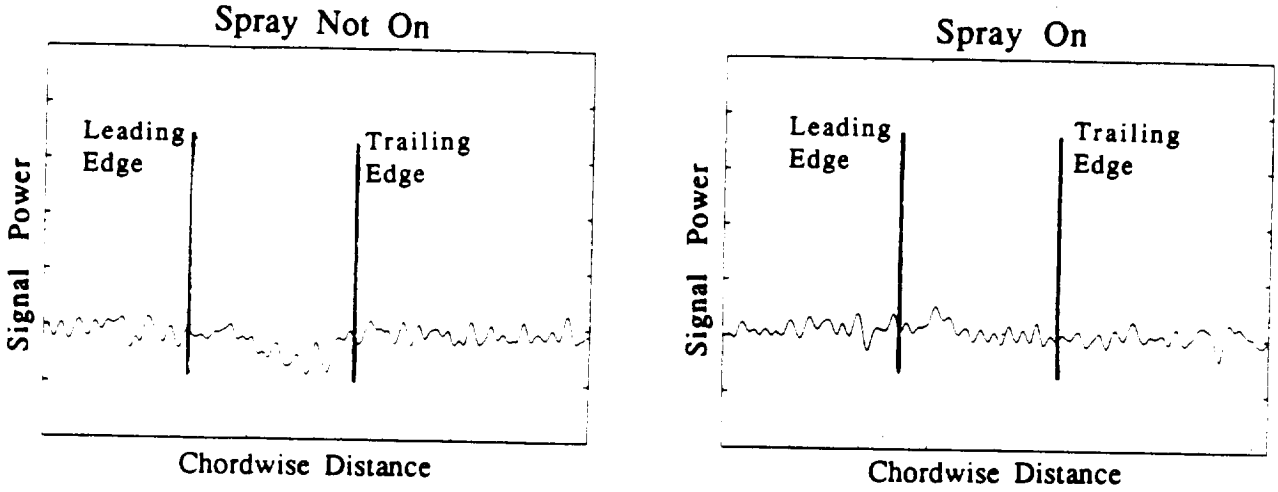

Figure 21. IR profiles at T=-0.9° C

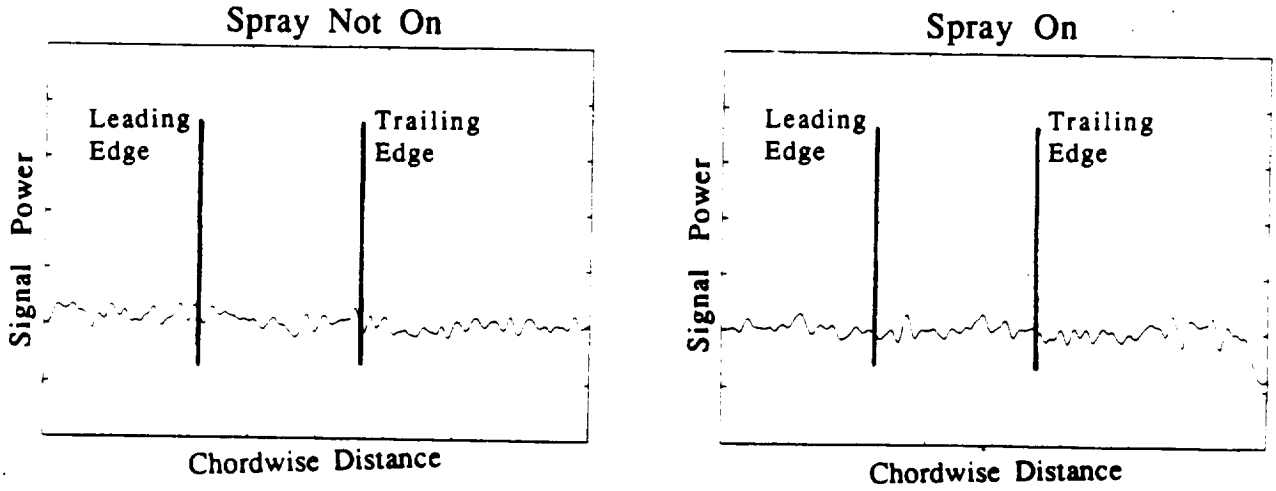

Figure 22. IR profiles at T=-0.3° C

Figure 23 demonstrates the effect of angle of attack on the characteristic icing signature. As the angle of attack is increased the icing region is expanded. That phenomenon is due both to the increased collection efficiency, over a wider area, and the shift in geometry, that exposes more of the icing region to the detector. That change is shown in Figure 24 These are all cold rime cases in the range of -17.2°C (1.0°F) to -18.4°C (-1.1°F) with an LWC of 0.17 g/m^3, and they all exhibit the expected characteristic profile. The amplitude of the signal measured at the high 10° angle of attack is smaller than that of the lower angles. This may be due to the spray nozzle being on the pressure side of the rotor, so that at high angles of attack more droplets are deflected away from the rotor, lowering the effective LWC, so there is less ice growth, or it may be do to calibration effects. Going from an angle of attack of 0° to 5° to 10° the heating region clearly becomes broader.

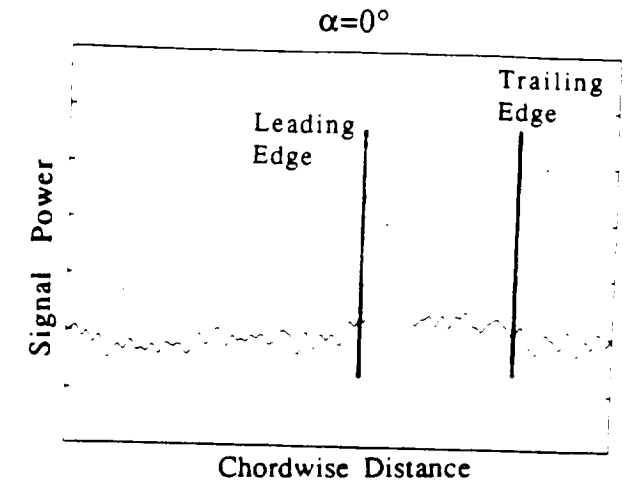

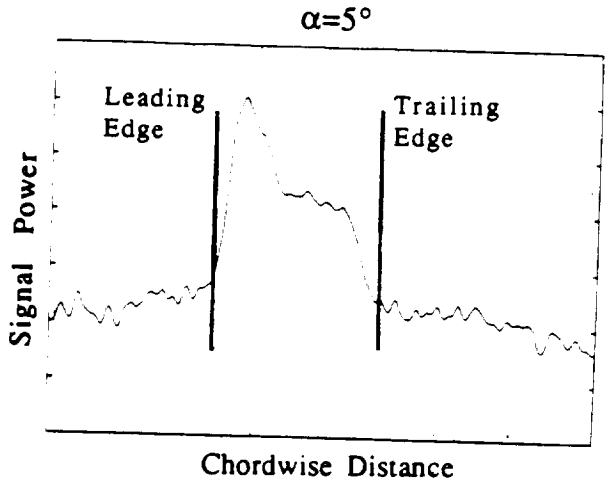

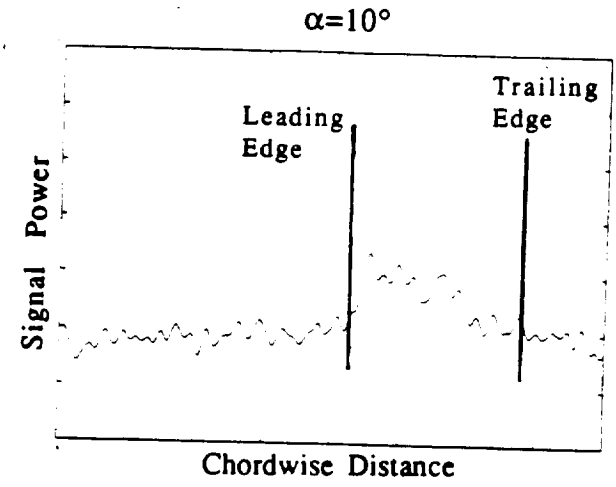

Figure 23. Change in angle of attack

6. Implementation Issues

While the rotor icing experiments demonstrate the potential for remote IR ice detection there are still several implementation issues to be considered, for flight applications. Some of these questions are addressed in this chapter.

6.1. Detector Focus

The simple rotor model, used for system demonstration in Chapter 5, did not include blade flapping or significant blade bending, which are both important effects in helicopter rotors. These effects, in a helicopter application, will make it more difficult to track the blade location, and to maintain focus. This may be addressed by use of a wide depth of field, or use of an auto focus system referenced to the blade leading edge.

The issue of accurate focus raised questions about its significance. During the tests discussed in Chapter 5 the detector was focused to give the sharpest profile possible. Although this detector was not designed to have a wide depth of field some experiments were conducted in order to determine the effects of out of focus operations, which might be due to such effects as blade flapping. Figure 24 presents a pair of profiles taken at T=-11°C (12.2°F) and a 5° angle of attack. The plot on the left is in focus. In the plot on the right the focal length was adjusted to intentionally defocus the image by moving the plane of focus from the rotor (35.0 cm (13.8 in) from the lens) to a point 6.5 cm (2.56 in) closer to the lens. As can be seen by comparing these profiles a significant change in focus has only a minor effect on the signal. This is not surprising as the detector gives a reading that is an

average over the spot size. The major effect of changing the focus is to slightly change the spot size. Therefore detector focus does not appear to be a critical issue.

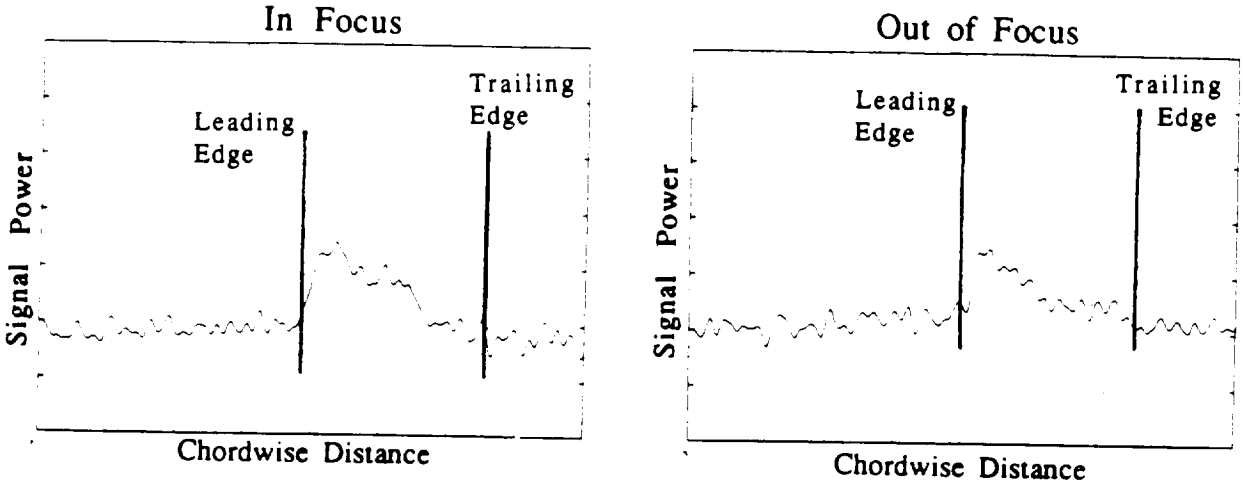

Figure 24. Comparison of out of focus and in focus profiles

6.2. Detector Icing

In order to test the effect of ice on the detector lens the dry nitrogen lens anti-icing system was disabled. Measurements were then taken with some ice or frost on the lens. Figure 25 is a pair of profiles that were taken with a layer of ice, approximately 1 mm thick, on the lens. The conditions for this measurement are a 5° angle of attack, an LWC of 0.17 g/m^3 and a temperature of -15.3°C (4.5°F). As can be seen the detector still functioned, however with significantly reduced signal strength.

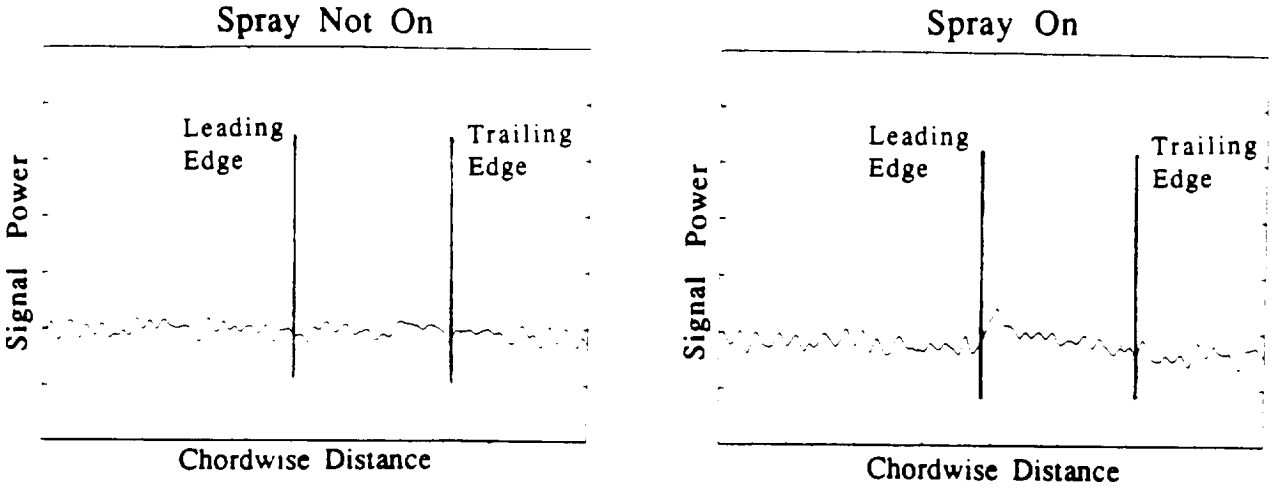

Figure 25. IR profiles taken with 1 mm of ice on the lens

In a flight application it will be necessary to prevent the pyrometer from icing, frosting, or becoming wet. It may be possible to simply shield the detector from the icing cloud to prevent detector icing. This can be accomplished if the detector optics can be kept out of the airflow, for example by putting them in a long tube perpendicular to the flow. Additionally a protective, IR transparent window, such as fused silica, could be put over the detector, and heated in cycles to deice it, however background signal problems must then be addressed.

6.3. Signal Processing

Several methods were considered for the signal processing necessary to automatically recognize the representative icing profile. The signal processing system must be able to detect ice from the detector output signals, which can be noisy and of a small amplitude, for some icing conditions. A simple threshold detector, even if it is calibrated to reject any DC offset, may have difficulty separating the signal from the background noise. For this ice detector to be useful, a method must be employed that will allow simple reliable data to be presented to the pilot, or to the automated deicing system.

The signal processing method that proved most effective in the preliminary testing that was done, was to convolve the IR signal with the expected chordwise temperature profile. The convolution produces a large amplitude at points where the test signal shape matches well with the expected profile, thus indicating the presence of icing. When there is a drop in the temperature profile, as might occur when there is a cold region on the rotor blade, then the test signal and the expected profile can be the inverse of each other. The convolution in this case will have a lower amplitude, or negative value, at that point.

In order to develop a generic chordwise temperature profile the unfiltered icing regions, the leading edge area where significant heating occurred, from three different known icing cases were averaged together. Cold cases were used, where there was a strong, distinct, icing profile. This "know icing profile" is shown in Figure 26. This profile still contains some high frequency noise, so the convolution with a test signal also contained this noise. It was found that a simple half of a sign wave of the appropriate width of the icing region was a more effective signal to convolve with. As this function has no high frequency components, the convolution additionally has the effect of low pass filtering the signal. This "smooth icing region" is shown in Figure 27.

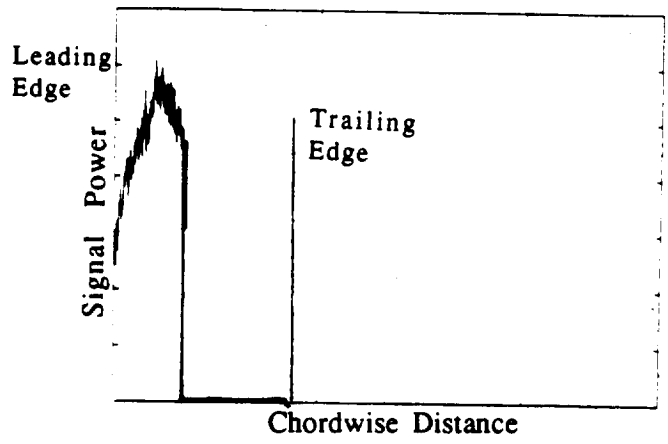

Figure 26. Average of the icing regions of three icing cases

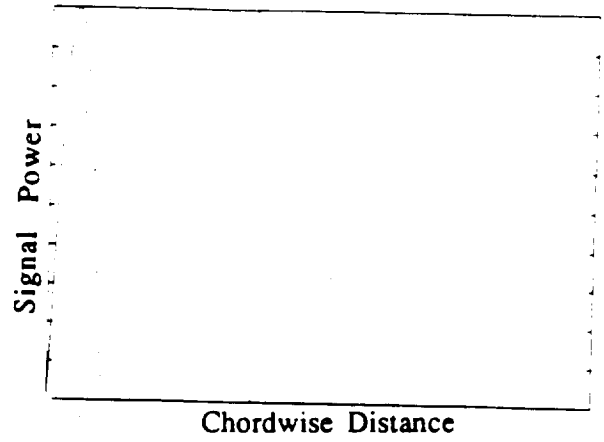

Figure 27 Half sine wave used as "Smooth icing region"

Figure 28 is an example of an unfiltered cold icing case at a temperature of -17.2° C (1.1°F), that was shown earlier in Figures 16 and 17. This signal was convolved with the "smooth icing region" to demonstrate this convolution method and the results are shown in Figure 29. As can be seen the convolution is of a large amplitude just aft of the leading edge, in the case with the spray on, thus the two signals are well matched in that region, indicating the presence of an ice accretion region.

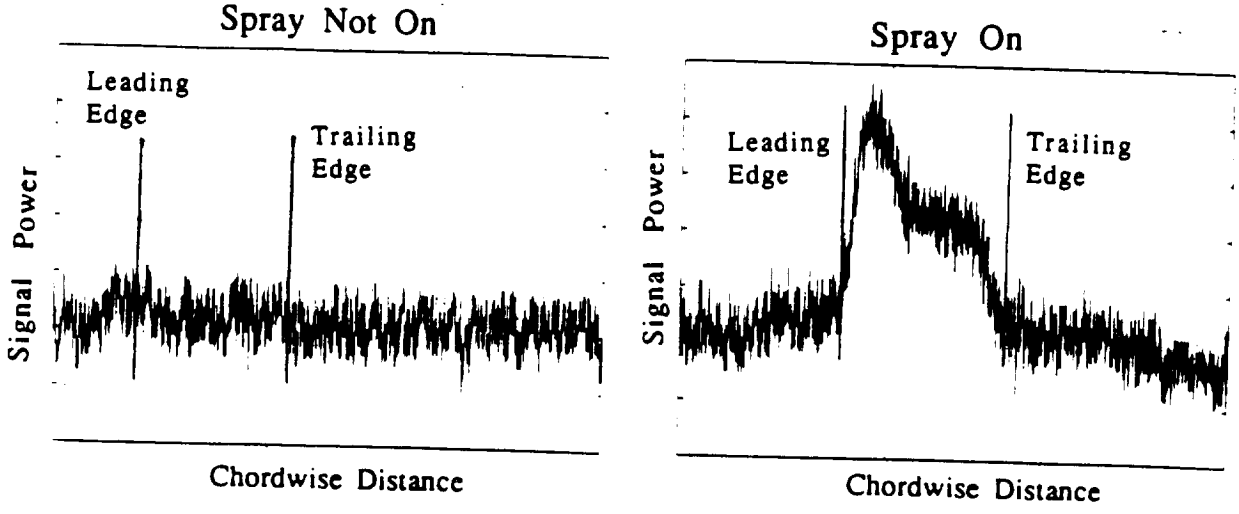

Figure 28. Unfiltered cold case with T=-17.2° C

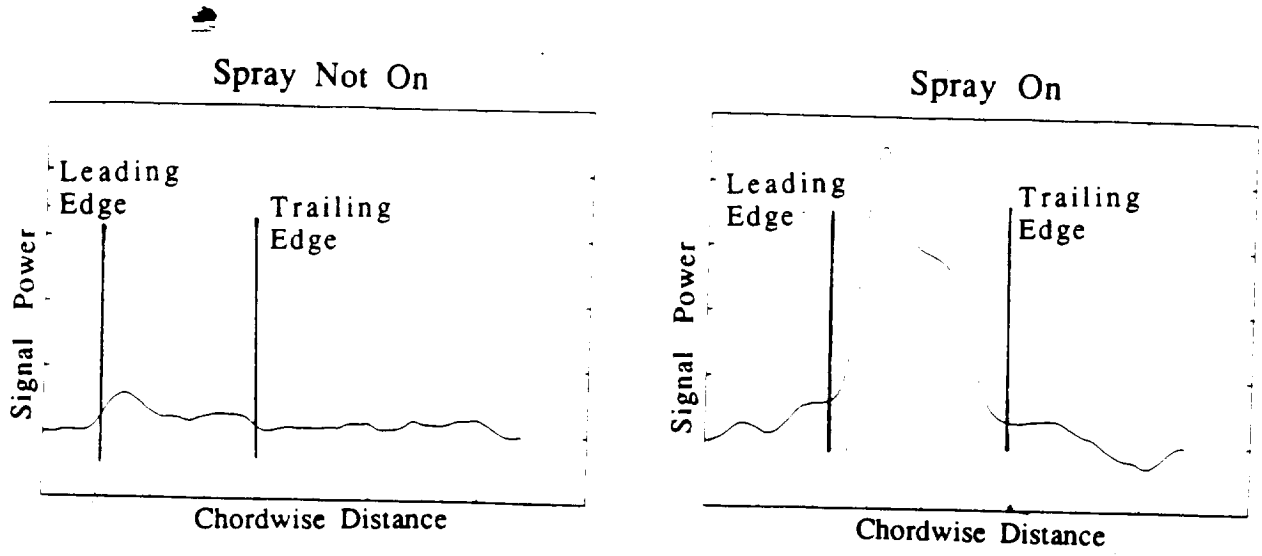

Figure 29. Convolution of cold icing case (Fig 28) with "Smooth icing region" (Fig 27)

Figure 30 is an example of an unfiltered icing case, at a temperature of -1.5°C. At these warm conditions there was a minimal amount of ice formed. It is clearly difficult to detect ice by simple inspection. This signal was convolved with the "smooth icing region" and the results are shown in Figure 31. As the convolution is of a large amplitude just aft of the leading edge, the convolution clearly makes the icing profile, in this difficult case, much easier to detect. Additionally in the case before the spray was turned on, the convolution, in the blade region, has a small value which makes the fact that the rotor blade was colder than the background standout.

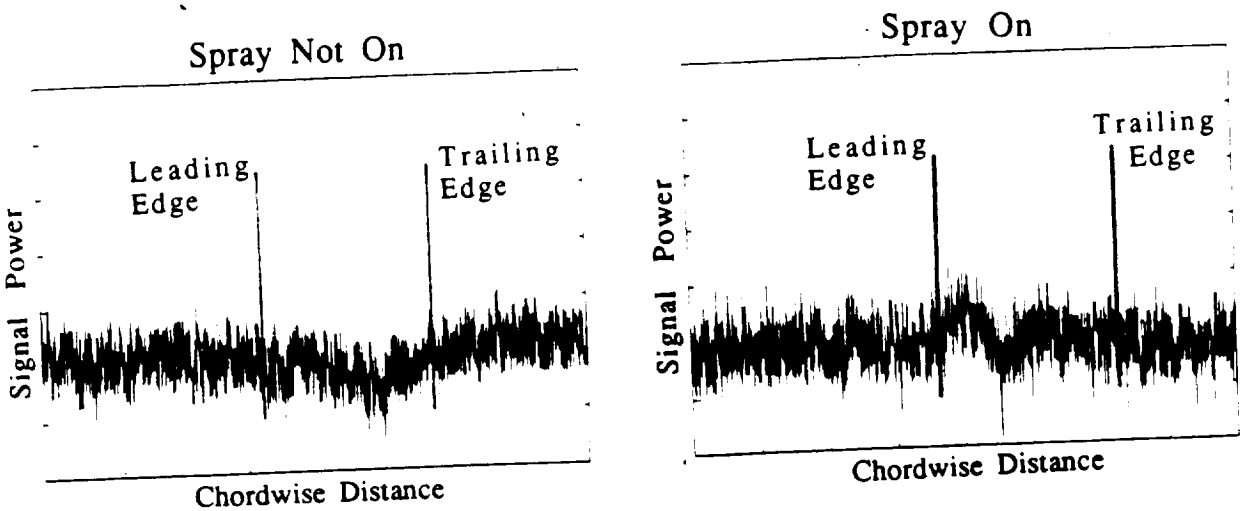

Figure 30. Unfiltered warm case with T=-1.5° C

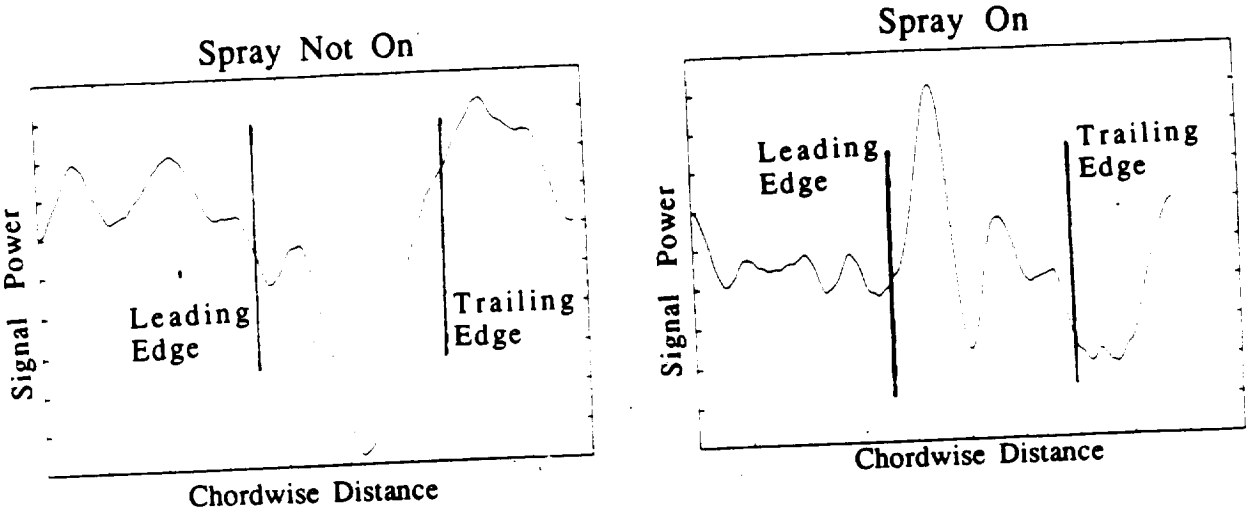

Figure 31. Convolution of warm icing case (Fig 30) with "Smooth icing region" (Fig 27)

Figure 32 represents a case taken at the same conditions as in prior case, however the temperature was warmed up to just above freezing, at a measured temperature of -0.5°C (3.1.°F). The unfiltered signal looked extremely similar to that of Figure 30. The convolution on the left shows, by the drop in the blade region, that the rotor blade was slightly colder than the background, before the spray was turned on. When the spray was turned on, as shown on the right, the convolution is approximately flat indicating that the

blade was isothermal, signifying no ice formation. This was confirmed when the rotor blade was stopped and inspected

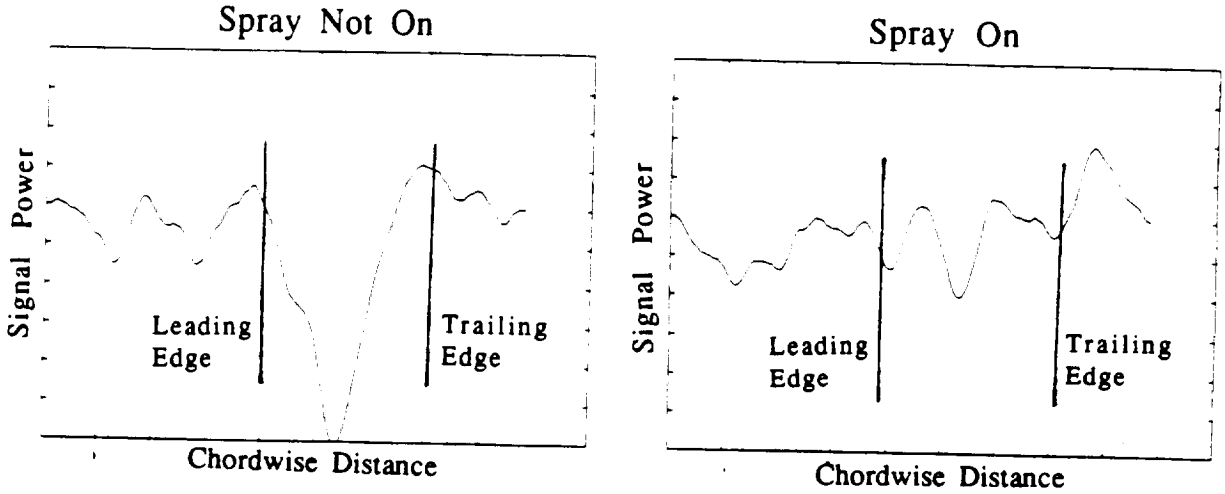

Figure 32. Convolution of warm no ice case with "Smooth icing region" (Fig 27)

For use in a production ice detector, some variations on this simple approach may be used. The detailed icing profile shape is a function of several variables including temperature, LWC and angle of attack. It may prove to be useful to measure several icing profiles, at different conditions. If the significant conditions are measured in flight then the appropriate profile, for the expected icing signal shape, may be selected, and convolved with the IR signal, to detect ice.

6.4. Detector Placement

Another issue to be considered is placement of the pyrometer on the helicopter. It will be necessary to mount the pyrometer so that it can view the blades, or possibly the tail rotor. Additionally, the possible problems of having the detector near a hot area such as an engine, or having it view through engine exhaust, could cause background radiation errors so must be considered. If the detector is designed so that it can aim at different spanwise locations it must be placed in a location where it can view all the span of the blade that is critical. Instead it is possible to use several different detectors, aimed at different spanwise locations.

It may also be useful to be able to monitor the tail rotor using the same detector. But, in most helicopters, this presents some difficulty in the placement geometry, because tail rotor placement, often affords no convenient mounting location perpendicular to the tail rotor plane.

6.5. Rotor Blade Tracking

Blade tracking is another issue to be considered. The convolution itself can provide some tracking information. If the location of the blade, in the signal profile, is well known, then it will be easier to convolve the IR signal to detect icing. Some of the background noise could otherwise be mistaken for rotor ice, without the proper tracking. Good tracking information will allow rejection of most of the signal, and allow only inspection of the part of the signal that contains the blade passage, for icing information. This will eliminate one cause of false positives, and can save computer time, that would otherwise be used to do convolutions on parts of the signal that do not contain the rotor blade. There are several possible ways to deal with blade tracking. It is expected that in most flight applications there will be sufficient contrast between the rotor blade, and the background that the signal itself will provide a reliable synchronization signal, after the convolution.

If the background matches the blade temperature, then some other method will be necessary to track the blade. A simple switch on the rotor shaft, will be able to give some synchronization signal. But as helicopter rotor blades have a free lead-lag hinge, this switch will not be able to give precise position information. It may be able to give enough general position information to reject some noise from the prior method and to significantly narrow the signal region to be searched to find the blade temperature profile.

Another possible method is optical. It may be possible to use a simple passive optical detector to detect the blade passing over the detector. While this method would work during the day, it is questionable for night use. Instead it may be necessary to augment such a

system by pointing a laser up, parallel to the ice detector, and detecting the reflected light to indicate blade passage.

The other method that could be used, is an infrared marker on the rotor blade. If a target is put at the trailing edge, with an extremely low emissivity, then it may be possible to detect that target, using the ice detector, as it would appear as a cold spike in the temperature profile. That spike can then be used to synchronize the ice detection process.

7. Conclusion

The problem of rotor ice detection was studied. Several different detection methods were considered, and the remote passive infrared method appeared to be the most promising. In this method the leading edge temperature of the rotor blade is monitored using an infrared pyrometer. During icing the latent heat of fusion of the supercooled water, is released, resulting in heating of the icing region. This theory was first verified using LEWICE ice accretion code.

In order to further substantiate the passive infrared method several experiments were run. Tests were run first on a static airfoil in the NASA IRT, using an infrared video camera, and thermocouples, to measure the icing region temperature. This experiment successfully demonstrated both the expected temperature profiles during the icing encounters, and the ability to monitor them remotely.

Following this successful demonstration, a prototype detector was designed and built, for use in rotating tests. It was mounted in a freezer, along with a small scale rotor and a spray apparatus, and was used to monitor ice accretion on the rotor. Again the expected icing temperature profiles were measured. The prototype proved effective at remotely detecting even trace ice on the rotating airfoil, with the appropriated signal processing. Several implementation issues were also considered and discussed. With a suitable implementation this prototype detector should also be able to detect ice on a full scale helicopter, in flight, as effectively. The method should therefore be considered for use on any rotorcraft that may encounter an icing environments.

References

[1]Heinrich, A. Ross, R. Zumwalt, G., Provorse, J., and Padmanabhan, Aircraft Icing Handbook - Vol. I, DOT/FAA/CT - 88/8-1, March 1988.

[2]Ibid. Vol II

[3]Ibid. Vol I

[4]Corley-Byrne, P.L., "Helicopter Icing and It's Measurement", Presentation at SAE subcommittee meeting AC-9C - Aircraft Icing Technology, October 1986.

[5]Hansman, R., Yamaguchi, K., Berkowitz, B., and Potapczuk, M., "Modelling of Surface Roughness Effects on Glaze Ice Accretion", AIAA-89-0734, AIAA 27th Aerospace Sciences Meeting, January 1989.

[6]Henry, R. and Guffond, D., "Application de la Thermographie Infrarouge a l'Interpretation d'Essais dans une Soufflerie Givrante", Societe Francaise des Thermiciens, January 1989.

[7]Skebe, S., "Synchronous Thermography", 3rd Japan-China joint conference on Fluid Machinery, April 1990

[8]Dershowitz, A., Hansman, R., "Passive Infrared Ice Detection For Helicopter Applications", American Helicopter Society, Washington D.C., May 1990

[9]Pau, L.F., El Nahas, M.Y. An Introduction to Infrared Image Acquisition and Classification Systems Letchworth, Herts, England: Research Studies Press; New York 1983

[10]EG&G Judson Solid State Products Catalog

[11]Hughes Aircraft Co. "Probeye Thermal Video System Series 4000 Operation Manual"

[12]Ruff, G.,Berkowitz,B. User Manual for the NASA Lewis Ice Accretion Prediction Code (LEWICE),NASA Contractor Report 185129, May 1990

[13]Dershowitz, A., Hansman, R. J., "Experimental Investigation of Passive Infrared Ice Detection for Helicopter Applications", AIAA-91-0667, AIAA 29th Aerospace Sciences Meeting, January 1991

[14]Hecht, E., Zajac, A. Optics, Addison-Welsley Publishing Co.

[15]EG&G Judson Solid State Products Catalog

[16]Janos Technology Inc. Precision Optics and Components Catalog

[17]Bete Fog Nozzle, Inc. Catalog